

Discovery of a Rare Late-Type, Low-Mass Wolf-Rayet Star in the LMC

BRUCE MARGON,¹ CATHERINE MANEA,^{1,2} ROBERT WILLIAMS,^{1,3} HOWARD E. BOND,^{3,4} J. XAVIER PROCHASKA,^{1,5}
MICHAŁ K. SZYMAŃSKI,⁶ AND NIDIA MORRELL⁷

¹*Department of Astronomy & Astrophysics, University of California, Santa Cruz, 1156 High St, Santa Cruz, CA 95064, margon@ucsc.edu*

²*Current Address: Department of Astronomy, University of Texas at Austin, Austin, TX 78712*

³*Space Telescope Science Institute, 3700 San Martin Drive, Baltimore, MD 21218*

⁴*Department of Astronomy & Astrophysics, Pennsylvania State University, University Park, PA 16802*

⁵*Kavli Institute for the Physics and Mathematics of the Universe, University of Tokyo, 5-1-5 Kashiwanoha, Kashiwa, Chiba 277-8583, Japan*

⁶*Warsaw University Observatory, Al. Ujazdowskie 4, PL-00-478 Warszawa, Poland*

⁷*Las Campanas Observatory, Carnegie Observatories, Casilla 601, La Serena, Chile*

(Received 2019 September 3; Revised 2019 November 4; Accepted 2019 November 22)

Submitted to ApJ

ABSTRACT

We report the serendipitous discovery of an object, UVQS J060819.93–715737.4, with a spectrum dominated by extremely intense, narrow C II emission lines. The spectrum is similar to those of the very rare, late-type [WC11] low-mass Wolf-Rayet stars. Despite the recognition of these stars as a distinct class decades ago, there remains barely a handful of Galactic members, all of which are also planetary-nebula central stars. Although no obvious surrounding nebulosity is present in J0608, [O II], [N II], and [S II] emission suggest the presence of an inconspicuous, low-excitation nebula. There is low-amplitude incoherent photometric variability on timescales of days to years, as well as numerous prominent P Cygni profiles, implying mass loss. There are indications of a binary companion. The star is located on the outskirts of the LMC, and the observed radial velocity ($\sim +250$ km s⁻¹) and proper motion strongly suggest membership. If indeed an LMC member, this is the first extragalactic late [WC] star, and the first with an accurately determined luminosity, as the Galactic examples are too distant for precise parallax determinations. A high-quality, broad-coverage spectrum of the prototype of the late [WC] class, CPD -56° 8032, is also presented. We discuss different excitation mechanisms capable of producing the great strength of the C II emission. Numerous autoionizing levels of C II are definitely populated by processes other than dielectronic recombination. Despite the spectacular emission spectra, observational selection makes objects such as these difficult to discover. Members of the [WC11] class may in fact be considerably more common than the handful of previously known late [WC] stars.

Keywords: stars: Wolf-Rayet — planetary nebula: individual — radiation mechanisms: general — stars: chemically peculiar

1. INTRODUCTION

During the UV-Bright Quasar Survey (UVQS) for intermediate-redshift QSOs bright in the far-UV (Monroe et al. 2016), several unusual stars also met the Survey’s *GALEX* (ultraviolet) and *WISE* (infrared) color-selection criteria, and were therefore observed spectroscopically (e.g., Margon et al. 2016). Here we report on another such unusual object, UVQS J060819.93–715737.4 ($l = 283^{\circ}$, $b = -29^{\circ}$, hereafter J0608), which has numerous intense emission lines of C II. This star is likely a new member of the extremely rare class of cool, late-type low-mass Wolf-Rayet (W-R) stars, a known but small collection of stellar objects whose spectra are dominated by extremely strong C II emission. Over half a century ago, one of us (HEB), while examining objective-prism plates from the Curtis Schmidt telescope at the Cerro Tololo Inter-American Observatory, discovered that CPD -56° 8032 (= Hen 3-1333, = V837 Ara) is an emission-line object having C II $\lambda 4267$ and $\lambda 6580$ as its strongest features (Bidelman, MacConnell, & Bond 1968). It

was suggested that the star could be an unusually cool WC-type W-R star. More detailed studies of the spectrum of this object are presented by Cowley & Hiltner (1969), Thackeray (1977), and numerous later authors.

It has been known for over a century that some central stars of planetary nebulae (PNe) have spectra that resemble those of classical W-R stars. An early example was BD +30° 3639 (= Campbell’s Hydrogen-Envelope Star; Campbell 1893), whose emission-line spectrum had been discovered on a Harvard objective-prism plate by Williamina Fleming, and announced by Pickering (1891). Campbell showed that the object is surrounded by a resolved, compact PN.

The modern understanding of classical W-R stars is that they are massive young stars with dense stellar winds. The W-R central stars of PNe, however, are a separate class of considerably less massive, older, and highly evolved objects, which also have dense outflows—as recognized as long ago as Smith & Aller (1971) in their discussion of Campbell’s Star, and in earlier papers which they reference. To recognize this fundamental difference, van der Hucht et al. (1981) suggested that the spectral types for low-mass W-R stars be enclosed in square brackets. Thus, for example, the carbon-rich, low-excitation spectrum of BD +30° 3639 is classified [WC9].

Webster & Glass (1974, hereafter WG74) suggested that CPD −56° 8032, along with PN M 4-18 (= PK 146+07 1), Hen 2-113, and possibly V348 Sgr, could be considered to be members of a class of objects with spectra dominated by strong C II emission. They appear to form an extension of the PN nuclei with WC spectra to even lower excitation levels than objects like BD +30° 3639. WG74 also pointed out that all four objects have strong infrared (IR) emission, implying a substantial dust component. Radial velocities, available for three of the objects, were all relatively large, indicating membership in an old disk or Galactic-bulge population. In the years since the WG74 paper, although many early [WC] stars have been found among PNe nuclei, only a few with late-[WC] spectra have been identified (Górny 2001; DePew et al. 2011).

The organization of this paper is as follows. We discuss our observations of the newly discovered object in §2, and the detailed nature of the spectrum in §3. The spectral-energy distribution is examined in §4, and inferred evolutionary status of the star in §5. Comments are made on the possible relationship to PNe in §6 and inferences from photometry in §7. The interesting absorption-line system is discussed in §8, a detailed description of the physics of the C II emission appears in §9, and conclusions are summarized in §10.

2. OBSERVATIONS

J0608 is noted by Monroe et al. (2016) as a Galactic source (i.e., not an AGN), without further comment. Based on good positional coincidence, we conclude that the star also appears in the *IRAS* (IRAS 06091–7157) and *AKARI* catalogs, as well as in *WISE* and *GALEX* (required for UVQS selection), again without comment. The bright IR fluxes suggest a dusty local environment.

The UVQS spectrum of J0608 was obtained on UT 2015 February 14 with the Boller and Chivens spectrograph at the 2.5m du Pont telescope of the Las Campanas Observatory. A 180 s exposure with the 600 l mm^{−1} grating blazed at 5000 Å and a 2'' slit yielded ~ 4 Å spectral resolution. The data were sky-subtracted and extracted with standard, optimal techniques. Although we suspect the presence of underlying nebulosity (see §6), as we have no knowledge of the morphology of any extended component (other than it is quite compact), we cannot quantitatively assess its contribution to the integrated spectrum. If low-level nebulosity exists, it would have been subtracted as if it were sky, but this is expected to be a small effect. Approximate flux calibration was obtained via observations of spectrophotometric standard stars. A finding chart and FITS format file of the spectrum are available in the MAST archive of UVQS data,¹ although the suggested line identifications and derived redshift there presume a QSO, and thus should be ignored.

The observed flux indicates $V \simeq 15.2$ at the time of that exposure, although uncertain light losses at the slit require that this estimate be used with caution. At $b = -29^\circ$, the anticipated interstellar extinction is modest; the *GALEX* catalog estimates $E(B - V) = 0.09$. Photometry from SkyMapper DR1 (Wolf et al. 2018) yields $r = 15.63$, $(g - r) = -0.14$, $(u - g) = -0.16$, $(r - i) = -0.19$.

The unusual nature of J0608 in the UVQS spectrum prompted us to seek considerably higher signal-to-noise spectra with better resolution, using the Magellan Echelle Spectrograph (MagE) on the Baade Magellan telescope (Marshall et al. 2008). Multiple exposures totaling 4,200 s were obtained on 2017 December 30, using a 1'' slit which provides ~ 1 Å spectral resolution. A second spectrum was obtained on 2019 May 3 with a similar configuration. Flux calibration was obtained via observations of multiple spectrophotometric standard stars, but must be regarded as approximate.

¹ https://archive.stsci.edu/prepds/uvqs/target_pages/j060819.93-715737.4.html

The two spectra are qualitatively similar; the 2019 spectrum is displayed in Figure 1. The changes in intensity between the two spectra are consistent with the differences in the signal-to-noise ratios and standard star calibrations, but do not rule out changes in the physical conditions in the wind between the two epochs of observation.

3. THE SPECTRUM OF J0608

Several unusual features of J0608 are readily apparent in Figure 1. The strongest emission lines prove to be due to C II, perhaps not immediately familiar to many stellar spectroscopists, with $\lambda 7236$, $\lambda 6580$, $\lambda 4267$ dominating the entire spectrum. Other prominent emission lines include narrow H α and H β (but not the higher-order Balmer lines), as well as numerous He I features, O I $\lambda 7773$, $\lambda 8446$, and prominent nebular lines, including [O II] $\lambda\lambda 3726, 3729$, [N II] $\lambda 6548, \lambda 6583$, and [S II] $\lambda 6717, \lambda 6731$. There are also numerous absorption lines; many but by no means all have P Cygni profiles. A list of suggested line identifications, together with equivalent widths and relative intensities in the two spectra, is given in Table 1. For lines which are purely in emission or absorption, wavelengths and equivalent widths are derived using the ALIS software package (Cooke et al. 2014), which includes a fit to the local continuum. This package employs a χ^2 minimization procedure to minimize the residuals between the data and a user-specified model, weighted by the inverse variance of the data². For lines with P Cyg profiles, the quoted wavelength is where the emission and absorption components transition into each other at the level of the continuum. As this object is known to be photometrically variable (see §7), and we have no accurate photometry contemporaneous with either of the two spectra, any apparent differences in flux between the two data sets in Table 1 should be regarded with caution.

It is clear from Table 1 that the emission lines display a substantial and consistent significantly positive radial velocity. For example the mean of the 110 strongest identified emission lines in the 2017 spectrum is $+247.1 \pm 1.4$ km s⁻¹, where the quoted uncertainty is the mean standard deviation. There is a small but formally statistically significant difference in the absorption-line radial velocity (excluding P Cyg absorptions), measured from 39 lines, of $+217.6 \pm 4.3$ km s⁻¹. An obvious blue continuum excess is also evident, consistent with the NUV and FUV detections by *GALEX*, as well as the marked UV-excess in the SkyMapper photometry.

The precise sub-classification of the very latest-type [WC] stars is somewhat author-dependent, hardly surprising given the paucity of class members. The topic is well-discussed by Crowther, De Marco, & Barlow (1998), de Araujo et al. (2002), Acker & Neiner (2003), Weidmann & Gamen (2011), and references therein. Today the latest, lowest-excitation end of this sequence is typically although not universally denoted as [WC11], and while we recognize that any sub-classification of J0608 will not be embraced unanimously, for the sake of brevity and specificity we will henceforth also refer to this object as [WC11]. The lack of both C IV and He II emission in J0608 comports well with the [WC11] class definition of Crowther et al. (1998). J0608 may well be one of the lowest-excitation [WC11] examples known, as our observed C II $\lambda 4267$ /C III $\lambda 5696$ ratio is more extreme than other published examples of late-type [WC] stars, including the prototype CPD $-56^\circ 8032$ (de Araujo et al. 2002), and more recently discovered low-excitation examples (Peña 2005).

As we are aware of no published, modern, broad-coverage digital spectrum of the prototype CPD $-56^\circ 8032$, for comparison we present one in Figure 2, kindly obtained by P. Massey, also with MagE at the Magellan telescope. J0608 clearly has a strong spectral resemblance, although CPD $-56^\circ 8032$ lacks the extreme blue continuum excess.

It has been suggested by Crowther et al. (1998) that V348 Sgr be removed from the already small class, due to the absence of C III $\lambda 5696$, which is indeed also weak, although definitely present, in emission in J0608. However, V348 Sgr is widely acknowledged to be an R CrB star, with violent and repeated photometric variability, behavior known to be absent in J0608 (cf. §7). Similar discussions appear in the literature regarding HV 2671 in the LMC (De Marco et al. 2002), and the more general question of a possible link between [WC11] and R CrB stars is intriguing but unsettled (Clayton et al. 2011).

4. THE SPECTRAL-ENERGY DISTRIBUTION

As substantial photometry is available for J0608 from the UV through the IR, the overall spectral-energy distribution (SED) of the object is clearly of interest, and is displayed in Figure 3, with two different extinction cases considered. In addition to the previously noted UV excess, there is a distinct IR excess. Because the object is known to be at least a low-amplitude photometric variable, and these data are not contemporaneous, caution must be taken interpreting the photometry.

² <https://github.com/rcooke-ast/ALIS>

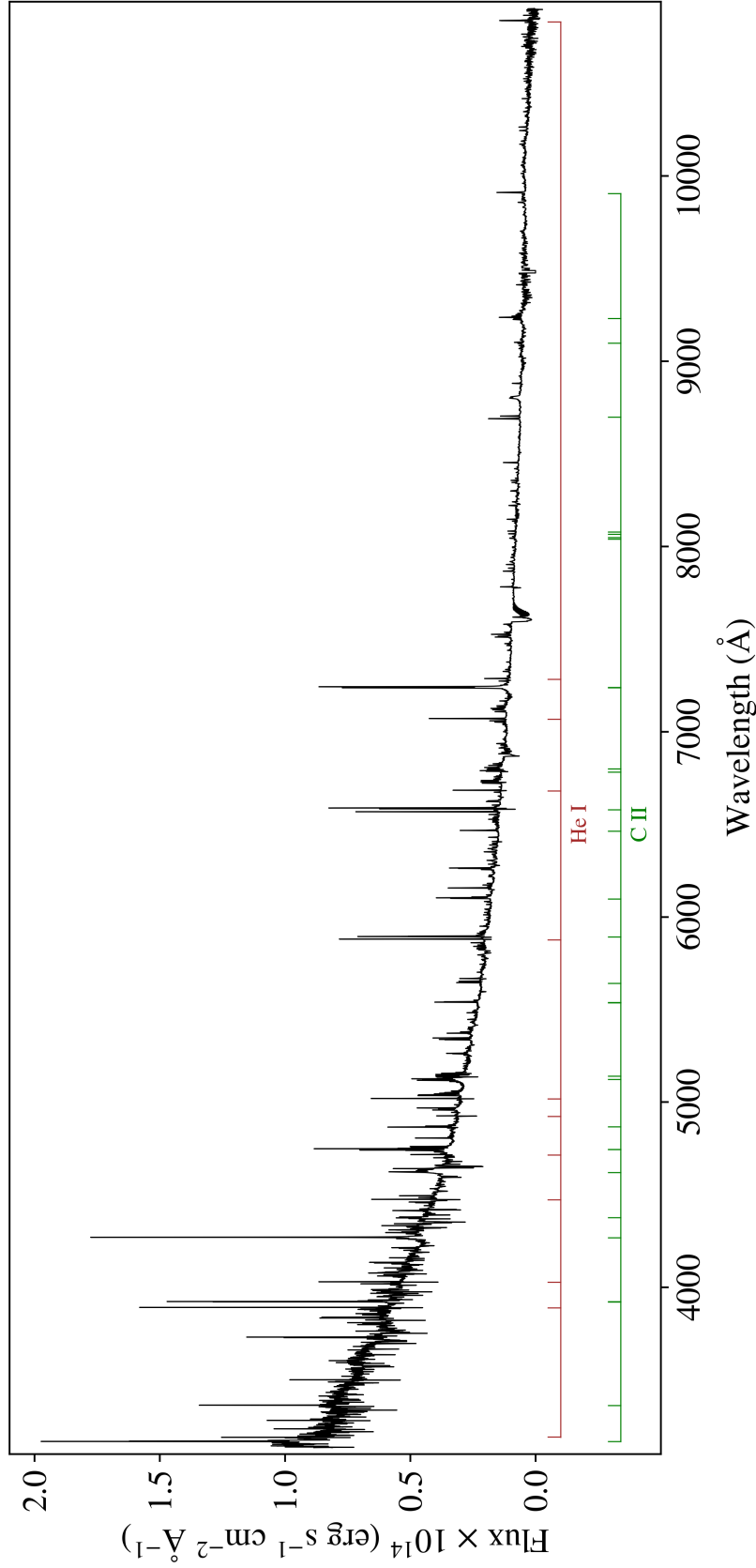


Figure 1. A Magellan MagE spectrum of J0608, obtained in 2019 May. The spectrum is dominated by C II $\lambda 4267$ and $\lambda 7231$ emission, but numerous other C II and He I emission lines are also indicated. Note the marked blue excess in the continuum, the P Cygni absorption profiles on many of the emission lines, and the marked increase in the occurrence of absorption lines shortward of ~ 5200 Å. Although not obvious in this figure, at the two extreme ends of the spectrum prominent emission lines of the C II $\lambda\lambda 3165, 3167$ doublet and He I $\lambda 10830$ are also well detected. Suggested line identifications are given in Table 1.

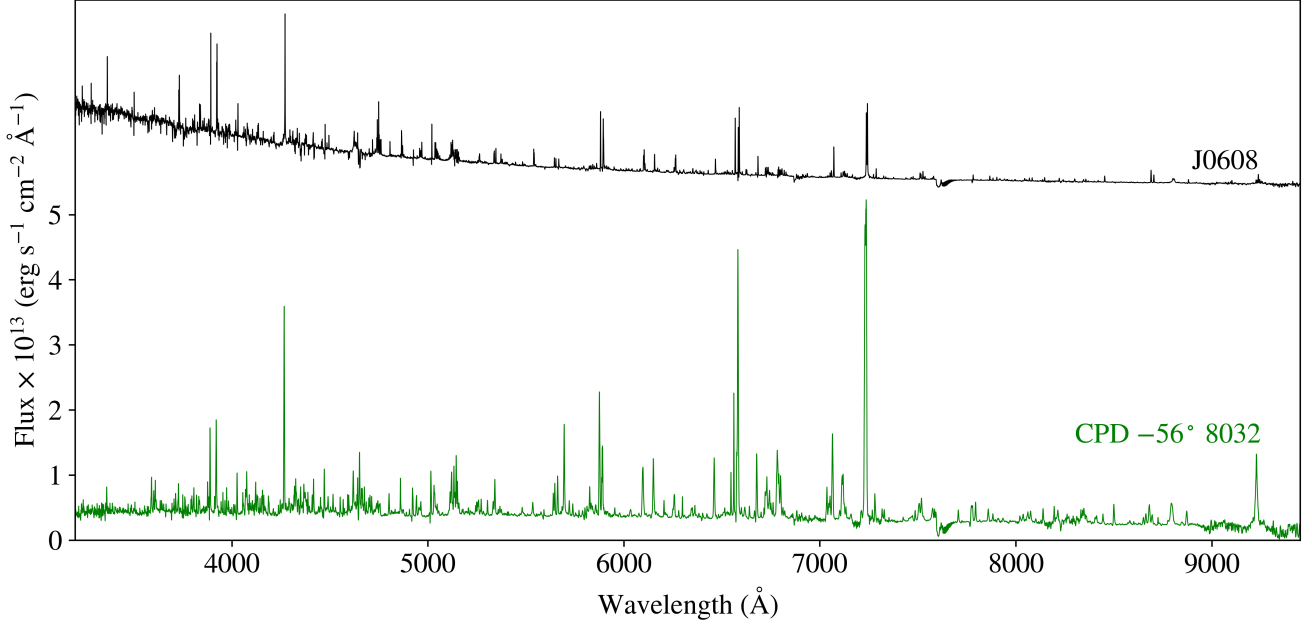


Figure 2. *Lower:* Spectrum of CPD -56° 8032, the [WC11] prototype, also obtained with Magellan and MagE on 4 February 2018, courtesy of P. Massey. *Upper:* The spectrum of J0608, reproduced from Fig. 1. This J0608 spectrum has been multiplied by a constant and then additively shifted upwards for clarity of display; absolute flux values can be obtained from Fig. 1. The similarity of CPD -56° 8032 to J0608 is evident, although the steep blue continuum of the latter star is missing, possibly due to circumstellar dust (Aitken et al. 1980, Kameswara Rao et al. 1990).

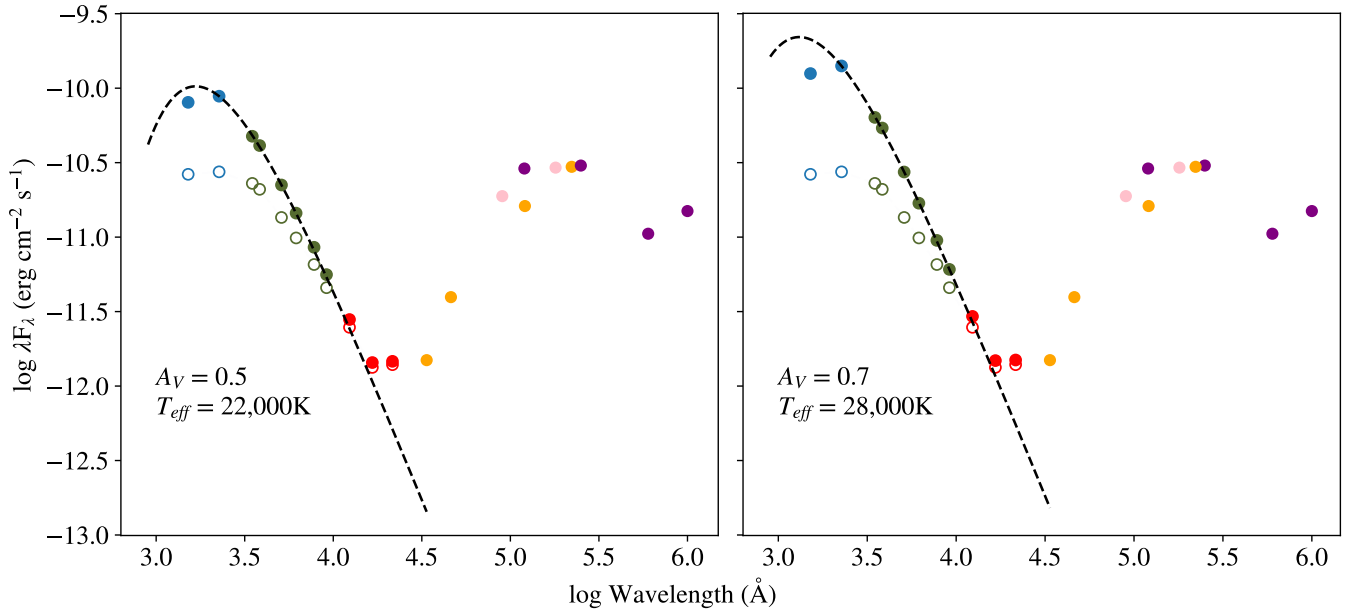


Figure 3. The spectral-energy distribution of J0608, utilizing data from *GALEX* (blue points), *SkyMapper* (green points), *2MASS* (red points), *WISE* (orange points), *AKARI* (pink points), and *IRAS* (purple points). Two extinction-corrected cases are considered, with parameters described in the text. *Open circles:* raw photometry; *filled circles:* extinction-corrected data. Plausible blackbody fits to the UV and visible data (*broken lines*) have $T_{\text{eff}}=22,000\text{K}$ (*left panel*) and $28,000\text{K}$ (*right panel*), but these fits are not unique. The infrared data are clearly in excess of the flux from the hot source, and this excess is likely due to circumstellar dust, ubiquitous in late [WC] stars. Note that none of the data sources are contemporaneous.

The rising blue continuum and the prominent *GALEX* detections indicate the presence of a hot source. As a very crude temperature indicator, we fit blackbodies to the UV and visible photometry. For this purpose, the blue and UV observed fluxes must be corrected for extinction. While the interstellar extinction in this direction is well constrained by a variety of data, and is small, the strong 2MASS and *WISE* detections in the IR imply that circumstellar absorption due to dust is also important, and quite possibly the dominant component of the total extinction.

We use the Fitzpatrick (1999) and Sun et al. (2018) models to correct the optical and UV data, respectively, and find that there is a range of A_V values that provide reasonable fits to the data of Figure 3. We show two examples, with $(A_V, T_{\text{eff}}) = (0.5, 22,000 \text{ K})$ and $(0.7, 28,000 \text{ K})$. We caution that these models are by no means unique solutions, and are also sensitive to the assumed value of R_V , the optical total-to-selective extinction ratio. The familiar value of $R_V = 3.1$, usually taken for the interstellar medium and assumed here, may not necessarily apply, due to substantial circumstellar extinction. Not surprisingly, T_{eff} is also extremely sensitive to the shortest-wavelength point, the *GALEX* FUV flux.

The bright IR components are certainly compatible with the marked IR excesses known to characterize the dusty late [WC] stars (WG74). The longest-wavelength points are clearly far in excess of the hot blackbody that creates the UV and optical emission. The mid- to far-infrared points cannot be fit with a single blackbody, but require multiple components in the $T_{\text{eff}} = 100 - 500 \text{ K}$ range. Again, these parameters should not be regarded as unique.

5. LMC MEMBERSHIP, HOST POPULATION, AND EVOLUTIONARY STATE

J0608 is located $\sim 5^\circ$ from the center of the LMC, but its $+247 \text{ km s}^{-1}$ emission-line radial velocity is nevertheless consistent with LMC membership (e.g., van der Marel et al. 2002). Nidever et al. (2019) and others have shown that LMC members extend well beyond the position of J0608. An alternative distance scenario placing J0608 in our Galaxy would require halo membership, in order to be compatible with the high radial velocity and moderately high Galactic latitude. However, the known Galactic late [WC] objects are fairly obviously not members of an especially old population, as they tend to be found at low Galactic latitudes.

The recent *Gaia* Data Release 2 (DR2) provides measurements of the parallax, π , and proper motion, μ , of J0608 and neighboring stars (Lindgren et al. 2016; *Gaia* Collaboration et al. 2018), allowing an opportunity to examine the issue of LMC membership. The DR2 parallax is $\pi = 0.0035 \pm 0.0321 \text{ mas}$, statistically consistent with an LMC distance ($\pi \simeq 0.020 \text{ mas}$), but also not ruling out membership in the distant Galactic halo. The DR2 proper motions of J0608 are $\mu_\alpha = 1.875 \pm 0.059 \text{ mas yr}^{-1}$ and $\mu_\delta = 1.028 \pm 0.068 \text{ mas yr}^{-1}$. These values are nicely consistent with *Gaia* data for LMC members (e.g., Helmi et al. 2018; Vasiliev 2018), whereas foreground Galactic-halo stars in this direction have a large dispersion in μ . These points are illustrated in Figure 4, in which *Gaia* proper motions for all stars within $2'$ of the location of J0608 are shown, as well as for two other fields of the same size, one closer to the center of the LMC, and one considerably farther, but at the same Galactic latitude. The LMC members are tightly clustered in proper-motion space, and J0608's proper motion lies well within this LMC distribution.

LMC membership for J0608 is nevertheless a bit surprising for two reasons. The LMC is well-studied and known to contain only early-type WC stars (e.g., Breysacher et al. 1999), a conclusion upheld even by the most recent surveys (Massey et al. 2017). Even the known LMC [WC] stars are only found to have spectral types of [WC8] or earlier (Peña et al. 1997; Crowther 2008). Moreover, the implied absolute luminosity of J0608 at the LMC distance, $M_V \simeq -3$, would exceed that normally quoted for the known Galactic [WC11] stars; however, luminosity estimates for the [WC11] subgroup are admittedly quite uncertain, as none are close enough for an accurate *Gaia* DR2 parallax. The known early [WC] stars in the LMC, where distance uncertainty is not an issue, are also all less luminous than inferred for J0608 if it is a member, despite their earlier spectral types (Peña et al. 1997). However, LMC membership may shed light on the marked weakness of C III $\lambda 5696$ emission in J0608: Torres et al. (1986) point out that all Galactic WC's have C III $\lambda 5696$ emission, but many in the LMC do not.

To investigate the host LMC population near J0608, we selected all stars in *Gaia* DR2 lying within an angular radius of $10'$ of the object, and with μ (in mas yr^{-1}) falling in the ranges $0.945 < \mu_\alpha < 2.445$ and $0.233 < \mu_\delta < 1.733$. These criteria provide a nearly pure sample of stars in the halo of the LMC at this location. In Figure 5 we plot the color-magnitude diagram (CMD) for these stars in the *Gaia* ($G_{BP} - G_{RP}$) color index and G apparent magnitude. The figure shows a well-populated giant branch with a pronounced red-giant clump, as well as main-sequence stars extending up to a color index of about zero.

To interpret this population, we have overlain the CMD data with theoretical stellar evolutionary tracks obtained from the MESA Isochrones and Stellar Tracks (MIST, version 1.2; Dotter 2016; Choi et al. 2016) website³ and its web interpolator. The MIST database includes calculations of magnitudes in the three *Gaia* bandpasses. We adopted MIST’s default stellar rotation of $v/v_{\text{crit}} = 0.4$, and obtained tracks for stars with initial masses of 1.0 to $3.0 M_{\odot}$, in steps of $0.5 M_{\odot}$. We adjusted the tracks to an LMC distance modulus of $(m - M)_0 = 18.48$ mag. After some experimentation, we found that we could fit the population reasonably well using a metallicity of $[\text{Fe}/\text{H}] = -0.75$ (appropriate for this location in the LMC halo) and a foreground extinction of $A_V = 0.3$ mag (consistent with the reddening discussed in §1).

Figure 5 indicates that there are stars as massive as $\sim 3 M_{\odot}$ at the site of J0608. We have also plotted, at the upper left of the figure, the location of J0608 itself as measured in *Gaia* DR2. For comparison with the theoretical tracks of normal stars, we would need to correct for the emission lines as well as for the substantial circumstellar extinction. These corrections—which we have not attempted in this initial discovery paper—would move J0608 to the left and upward in the figure. Its position would likely agree with the post-asymptotic-branch (post-AGB) tracks of the more massive stars in this population.

However, the high carbon abundance and likely hydrogen deficiency of J0608 strongly suggest that it is not in a normal hydrogen-burning post-AGB evolutionary state. Evolutionary scenarios for late [WC] objects like CPD -56° 8032 have been discussed by many authors, including Méndez (1991), Cohen et al. (1999), Crowther (2008), Górný (2008), Clayton et al. (2011), Guerrero et al. (2018), and references therein. These scenarios usually involve a helium thermal pulse during post-AGB evolution. If the pulse occurs as late as the beginning of the descent of the white-dwarf cooling sequence, the star will retrace its post-AGB evolutionary track—such as those shown at the top of Figure 5—back to the red-giant regime. Thus J0608 could now be returning from such an event—or possibly it is still on its way to becoming a “born-again” red giant. Alternative scenarios involving binary interactions have also been discussed (e.g., De Marco 2008; Clayton et al. 2011; Manick et al. 2015). We return to the question of binarity of J0608 in §8.

In summary, the radial-velocity, proper-motion, and parallax measurements make it appear likely that J0608 belongs to the LMC, and that it is descended from a star of initial mass possibly as high as $\sim 3 M_{\odot}$. The post-AGB evolution of stars this massive is very rapid, and J0608 is in a transient evolutionary stage of high, although not unprecedented, luminosity (cf. Schönberner 1981).

For the sake of completeness, we note that van Aarlie et al. (2011) have described two LMC stars that they suggest are of late [WC] spectral type; one is the well-studied HV 2671. Although their spectra do contain C II emission lines, they otherwise do not strongly resemble J0608, CPD -56° 8032, or other objects in the WG74 class. As in the case of V348 Sgr discussed in §3, we believe these may be more appropriately described as alternative objects such as R CrB

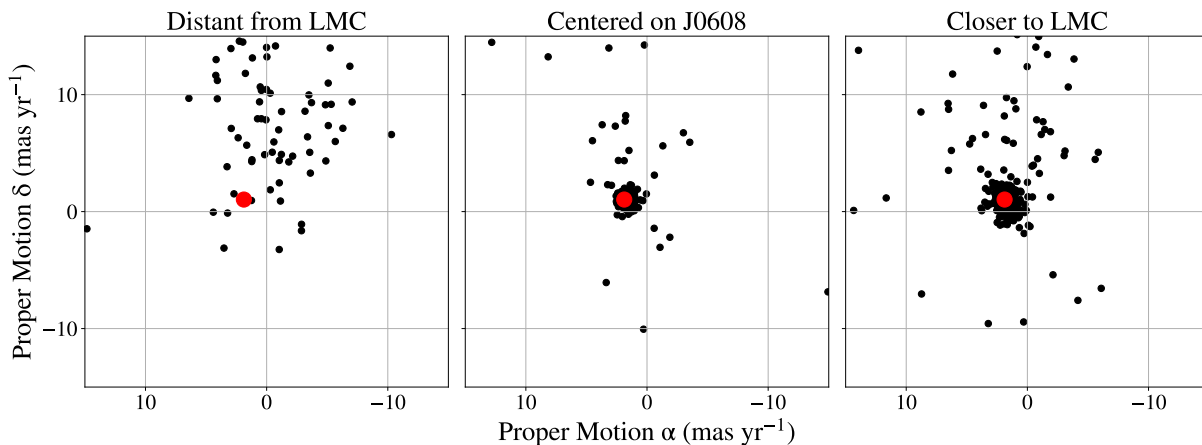


Figure 4. *Gaia* DR2 proper motions near J0608 and environs. *Center panel:* A square of $4'$ centered on J0608 (red dot). *Left panel:* $4'$ field $\sim 20^{\circ}$ from the LMC but at the same galactic latitude as J0608, presumably all halo stars; note the large scatter in the halo-star proper motions. *Right panel:* $4'$ field $\sim 3^{\circ}$ from the LMC center, dominated by LMC members. The observed motion of J0608 is superposed on the left and right panels. The motion of J0608 strongly implies LMC membership.

³ <http://waps.cfa.harvard.edu/MIST/>

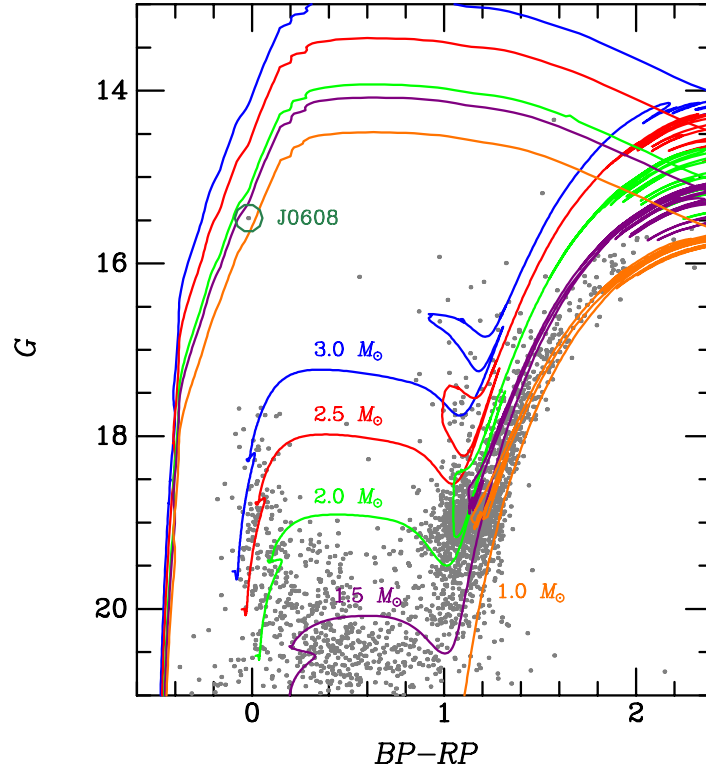


Figure 5. Color-magnitude diagram in the *Gaia* bandpasses of LMC stars within $10'$ of J0608 (*gray filled circles*), selected from *Gaia* DR2 data on the basis of proper motions as described in the text. Superposed (*colored lines*) are theoretical stellar evolutionary tracks from the MIST website, for initial masses of 1.0 to $3.0 M_{\odot}$, and adjusted to the extinction, metallicity, and distance of the LMC, as explained in the text. Also shown is the position of J0608 itself (*large green circle*), but it would need to be adjusted to the left and upwards for emission lines and circumstellar dust for comparison with the tracks. There are stars as massive as $\sim 3 M_{\odot}$ in this field, and the position of J0608 is consistent with it being descended from a fairly massive progenitor star, and now lying on a post-AGB track at high luminosity.

stars, in agreement with the classification already given for HV 2671 by multiple authors, e.g., Alcock et al. (2001), Soszyński et al. (2009), and Clayton et al. (2011). However, we do note that the second of the Aarlie et al. (2011) objects, J055825.96–694425.8, has been termed “likely a hot proto-PN or PN” by Hrivnak et al. (2015), although the spectrum presented by van Aarlie et al. (2011) appears to show prominent Mg *b* absorption, again in contrast to the WG74 objects.

6. RELATION TO PLANETARY NEBULAE

As all known Galactic late [WC] stars are surrounded by resolved PNe, one might wonder about the presence of a nebula associated with J0608, which might or might not be detectable at the LMC distance. J0608 is unresolved in SDSS r and narrowband $H\alpha$ filters at the $\sim 1''$ level on CCD direct images kindly obtained at our request by M. Phillips (private communication) on multiple nights at both the du Pont and Swope telescopes of the Las Campanas Observatory. Any nebula at this location must be reasonably inconspicuous, because this region has long been well surveyed for PNe (e.g., Morgan 1994 and references therein), and multiple LMC-member PNe (as well as clusters) are indeed known even at this relatively large offset. The PN MGPN LMC86 (Morgan & Good 1992), for example, is located just $18'$ distant, and is considerably fainter than J0608 (Leisy et al. 1997), perhaps leading one to wonder how the emission spectrum of J0608 has escaped previous attention, especially as there is no evidence for substantial photometric variability (see §7) that might have pushed it beyond the limit of detectability in objective-prism surveys. However, the photographic emulsion/filter combination used in the MG survey (IIIa-J/GG455) by misfortune excludes the prominent emission lines in J0608.

Through the kind assistance of N. Hambly, we have examined a digitized version of the AAO/UKST SuperCOSMOS $H\alpha$ Survey film (Parker et al. 2005) which includes J0608. No nebulosity is apparent on angular scales ranging from a few arcseconds to several arcminutes.

The J0608 spectrum does show the clear presence of [O II], [N II], and [S II] emission, quite possibly originating in a surrounding but inconspicuous nebula. The intensity ratios of the [O II] and [S II] doublets indicate electron densities in the region where these lines are formed to be in the low-density limits of both doublets, i.e., $n < 10^3 \text{ cm}^{-3}$. This suggests the presence of a low density circumstellar nebular gas that is separate from the much higher density wind. The absence of any [O III] $\lambda\lambda 4959, 5007$ emission in J0608 does not alter this inference—it is also absent in other members of the class known to host easily resolved, low-excitation planetary nebula (e.g., De Marco, Barlow, & Storey 1997; Henry et al. 2010). We have examined the two-dimensional MagE spectrum at the [O II] lines to search for spatial extension, and find none, but the modest seeing at the time of this exposure makes this result inconclusive. Finally, the observed intense *WISE* IR flux for J0608 indicates that it shares the same marked IR excess common to late [WC] stars, which are known PN central stars (e.g., Zijlstra 2001; Górny et al. 2001).

The lack of a detectable nebula in J0608, while disappointing, may not be surprising. Only a few LMC PNe have angular extent $>1''$, and the Galactic [WC11] nebulae, when extrapolated to the LMC distance, would be quite small in angular extent (e.g., De Marco et al. 2002; Chesneau et al. 2006).

7. PHOTOMETRIC VARIABILITY

Due to its proximity to the LMC, J0608 has extensive broad-band photometry in the OGLE III and IV surveys (Udalski et al. 2015). The majority of the data are in the I -band, with some additional V observations. The I -band data consist of observations on 946 nights in the 2001-2018 interval. Typical observations are shown in Figure 6. Over the long term, the object averages $I = 15.45$, but irregular variations of up to ~ 0.15 mag on timescales of days and weeks, well beyond the uncertainty in the measurements, are quite evident. The data were examined for periodicities in the $0\text{--}48 \text{ d}^{-1}$ range, but no significant periods were found. There are also ASAS-SN data (Shappee et al. 2014; Kochanek et al. 2017) on this star, exhibiting similar behavior.

Irregular variability of PN nuclei on a timescale of hours to days, as we observe here, has been reported for multiple objects (e.g., Bond & Ciardullo 1991; Handler et al. 2013) and is typically ascribed to a variable stellar wind. The existence of a wind in J0608 is also supported by the dust implied by the bright mid-IR flux noted above, as well as the prominent P Cyg line profiles.

Historical photometry of J0608 is available from the Harvard plate collection via the DASCH archive (Grindlay et al. 2012; Tang et al. 2013). There are several dozen points spanning a century, with reasonably densely sampled data from 1925 to 1950. The object averages $m_{pg} \simeq 15.3$, with no obvious variations beyond the ± 0.2 mag level. (With this statement we ignore a single highly discrepant, bright point, where inspection of the underlying image strongly suggests a spurious observation.) Although in limited, irregular sampling there is always the possibility of missing a sporadic event, this behavior is likely quite different from that of V348 Sgr, to which J0608 bears some spectral resemblance. The former star undergoes multiple dramatic (~ 6 mag) variation events (Heck et al. 1985), a signature of the R CrB class.

8. THE PHOTOSPHERIC SPECTRUM

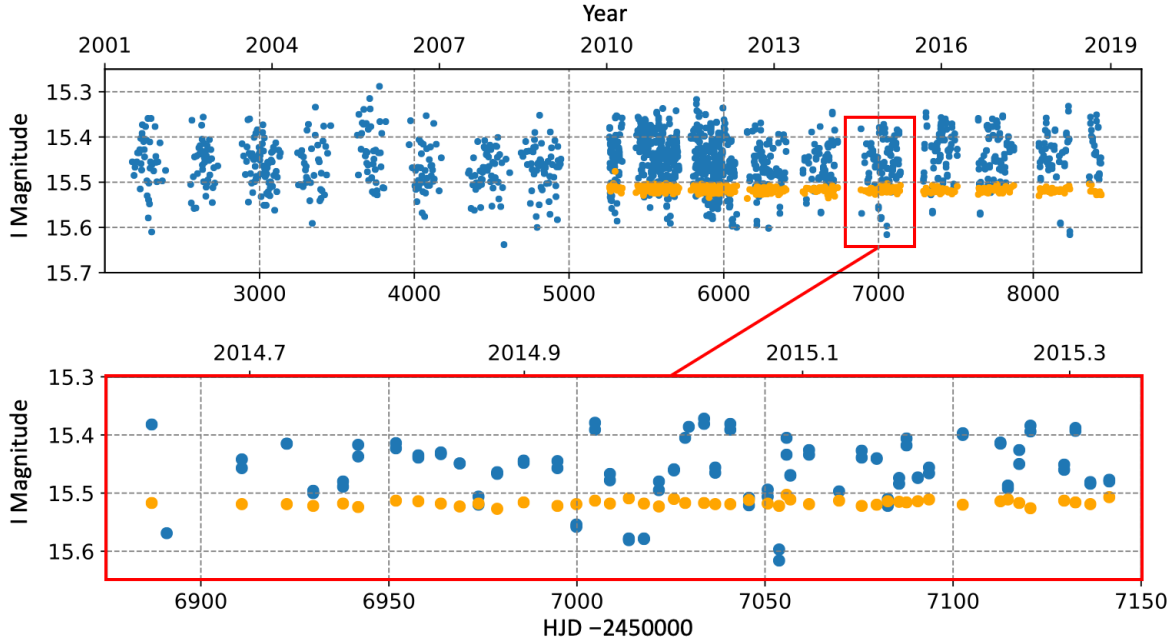


Figure 6. OGLE *I*-band photometry of J0608 (blue dots) and a nearby comparison star of similar magnitude (orange dots) makes it clear that J0608 has significant, chaotic flickering, on a timescale of days, presumably due to a variable wind. The enlargement (lower panel) is an arbitrary section of data intended to show more detail. Time series analysis uncovers no significant periodic behavior.

Although the spectrum of J0608 is dominated by the intense emission of C II and He I, which together with the associated P Cyg profiles are normally attributed to a wind, there are also spectral clues to the underlying star. Shortward of ~ 5200 Å, absorption lines become noticeably more frequent, and the P Cyg profiles are largely absent. We have identified these numerous absorption lines in the blue as He I and, remarkably, multiple Ne II and O II lines (Figure 7), which suggest the presence of a hot subdwarf. The spectrum (and blue continuum) well match the known characteristics of hot subdwarf stars, for example Heber (2001). The absorption lines are perhaps narrower than one might expect for a typical subdwarf, possibly indicative of the high luminosity inferred in §5, and lower surface gravity. Ne II absorption has been known in hot stars for almost a century (Menzel & Marshall 1933), and these lines are another signature of hot subdwarf stars (Schindewolf et al. 2018). The lack of absorption longward of 5200 Å is readily understandable. Such absorption multiplets exist but have low f -values, because they consist of absorption to S states, which have lower energy than the P and D states, and hence longer wavelengths. Our (admittedly crude) estimates of T_{eff} in §4 are also compatible with the hot-subdwarf hypothesis. In this scenario, the observed velocity differences between emission and absorption are due to the geometry of the star and its wind.

The colors of J0608 agree well with the large sample of hot subdwarf stars with *Gaia* parallaxes studied by Geier et al. (2019). The majority, although not quite all, of the stars in their sample are less luminous than we would infer for J0608 in the LMC. However, as discussed in §5, there are hot post-AGB stars that briefly pass through the required luminosity, and examples are certainly known in the field (Schönberner 1981).

Although the simultaneous presence of spectral lines of such disparate temperatures as seen in J0608 may seem odd, there is certainly precedent in the late [WC] stars. IRAS 21282+5050, for example, is found to have characteristics of both a [WC11] and also O7(f) (Cohen & Jones 1987, although the spectrum lacks C II $\lambda 4267$), and later classified simply as O9–O9.5 (Crowther et al. 1998).

An increasing fraction of PN central stars have been found to be binaries in recent years, but little is known about binarity in [WC] stars. Manick et al. (2015) report a spectroscopic binary in a [WC4] star, but failed to find evidence for binaries in multiple late-type [WC] stars similar to J0608. Miszalski et al. (2011) present more indirect evidence for the possibility that CPD -56° 8032 is a long-period (years) binary. We have compared our 2017 and 2019 MagE spectra of J0608 in a search for radial-velocity variability. The emission- and absorption-line mean velocities in the 2017

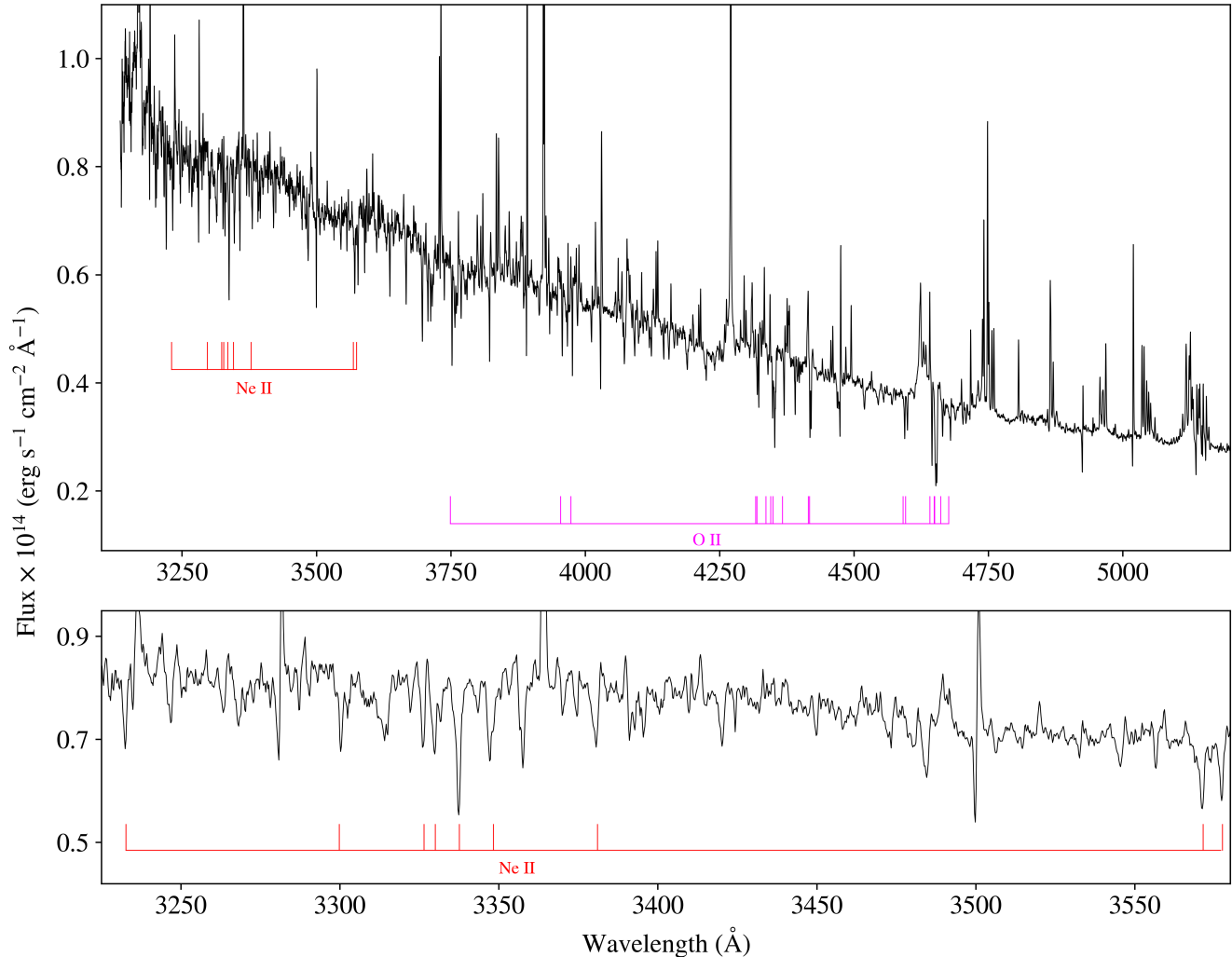


Figure 7. *Upper panel:* An enlargement of the UV/blue spectrum of J0608 to illustrate the numerous stellar absorption lines. Ne II and O II lines are marked. Most of the remaining absorption lines are He I. These data are identical to those of Fig. 1. *Lower panel:* A section of the spectrum encompassing the Ne II lines, yet further enlarged to show the profiles.

data have been quoted in §3. The analogous values from the 2019 spectra are $+232.1 \pm 1.5$ km s $^{-1}$ and $+211.6 \pm 3.2$ km s $^{-1}$, respectively. Thus in the time intervening between the two spectra, the velocity of the emission system has decreased by 15.0 ± 2.1 km s $^{-1}$, and the absorption system has decreased by a similar though not statistically significant amount, 6.0 ± 5.4 km s $^{-1}$. Therefore there is suggestive evidence for radial-velocity variability. Further radial-velocity monitoring is obviously desirable, and until variations are firmly detected, we cannot determine unequivocally whether J0608 is a single star or binary system.

9. THE REMARKABLE EXCITATION OF C II

Previous comments on the interesting physics of the intense C II emission in late [WC] stars have been made by several authors, e.g., Dahari & Osterbrock (1984), Leunhagen & Hamann (1994), and De Marco, Storey, & Barlow (1997). Although most authors attribute the lines to recombination (e.g., Kaler 1981), multiple other mechanisms are possible (Clegg 1989). Dahari & Osterbrock (1984), for example, briefly discuss resonance fluorescence pumping, which we further expound upon below.

The prominent emission lines in [WC] stars, which are formed in a stellar wind, differ from those of the emission spectra of gaseous nebulae, in that the strongest CNO lines are from high-excitation levels that are unlikely to be populated by collisional excitation. This is probably due to higher densities in the [WC] line-forming region compared

with those of most nebulae, so the forbidden lines are collisionally de-excited. In addition, and in contrast to nearly all other emission-line objects, many of the emission lines observed in [WC] spectra originate from autoionizing states of C II. A high abundance of carbon enables the normally weaker dielectronic recombination (DR) lines to be detectable in [WC] stars such as J0608, and an additional factor may be that excitation of the autoionizing levels may occur as a result of processes that are favored in stellar winds, such as radiative excitation, because the stellar radiation field is not diluted, as it is in nebulae.

Among the prominent emission features in the J0608 spectrum that do not belong to H, He I, or C II are O I $\lambda 7773$ and O I $\lambda 8446$, whose emission components have comparable strength and have been shown to be density diagnostics when they have comparable intensities. The upper level of $\lambda 8446$, a triplet, is highly populated by strong resonance fluorescence from Ly β scattering among excited O I triplet states (Bhatia & Kastner 1995). However, O I $\lambda 7773$ is a quintet, and with its high excitation potential the only way it can be excited at levels comparable to the $3p\ ^3P$ upper level of $\lambda 8446$ is by collisional transfer from that level to the $3p\ ^5P$ upper level of $\lambda 7773$, which requires densities $n_e \geq 10^{11}\text{ cm}^{-3}$ (Kastner & Bhatia 1995). In spite of the fact that the strong absorption component of $\lambda 7773$ is comparable to its emission component and thus causes the net line flux to be nil, the fact that the line is optically thick at its high excitation potential indicates that it is significantly coupled to the $3p\ ^3P$ level by high density. The primary line-emitting region of the J0608 wind may therefore be assumed to have densities in the regime of $n_e \geq 10^{11}\text{ cm}^{-3}$, in accordance with density values that have been inferred from studies of other late [WC] stars (De Marco & Crowther 1998).

An additional argument related to the density of the emitting region may be inferred from Balmer line intensities, inasmuch as recombination-line intensities for ionized gas at nebular densities are computed to have $I(H\alpha)/I(H\beta) \simeq 2.7$ over a wide range of temperatures and densities (Storey & Hummer 1995). It is seen from Table 1 that relative intensities are instead observed to be $I(H\alpha)/I(H\beta) \approx 2$ in both J0608 spectra, which are below the recombination value and therefore could be an indication of high densities, $n_e > 10^{11}\text{ cm}^{-3}$ (Drake & Ulrich 1980). However, it should be cautioned that a significant fraction of the H β emission feature may be due to C II $\lambda 4862.6$, which could have an intensity comparable to that of H β , based on the intensity of its companion multiplet member C II $\lambda 4867$. Thus, information about densities inferred from the Balmer line ratios is uncertain.

Detailed study of the spectrum of J0608 reveals that it is particularly complex. Like other [WC] stars, it shows an emission spectrum with prominent He I and C II lines, many of which have P Cyg profiles with absorption components that indicate significant optical depth in the lines. The Balmer series is present and stronger than the He I lines, but does not show appreciable absorption components as do the He I lines. The emission features are superposed on a quite blue continuum at visible wavelengths, and many of the C II emission lines can be identified as originating from quartet states of high excitation potential, with $\chi \geq 18\text{ eV}$.

The presence of observed quartet multiplets in emission is particularly interesting in that quartet levels of C II cannot be populated by either normal two-body radiative or DR of C III in its ground state because capture of a spin-1/2 free electron by the C III $2s^2\ ^1S_0$ singlet ground state can produce only C II doublet states. However, as noted by Dahari & Osterbrock (1984), DR can populate C II quartet states via the first excited (metastable) triplet level of C III, $2s2p\ ^3P^o$, following its excitation by collisional or photo-excitation from the 1S_0 ground state. DR is a resonant radiation-less process where the kinetic energy of the free electron must be the same as the potential energy of the doubly excited state that it occupies. This strict constraint on the free electron energy causes DR rates to be very sensitive to the electron temperature T_e .

Returning to the presence in the J0608 spectrum of C II lines from quartet levels that can be populated by DR, the high densities and the possible excitation of doublet levels by resonance fluorescence, both from the continuum and from scattering of He I resonance lines, raises the possibility that the dominant process populating C II autoionizing quartet levels may not be solely DR. At the densities in the line-emitting region, collisional transfer between bound doublet and quartet levels having similar excitation potentials should be strong, similar to the collisional process that couples O I $\lambda 7773$ to $\lambda 8446$.

Since collisional exchange between bound levels of C II is likely to be strong, the best means of determining the significance of DR in populating quartet states is observation of those emission lines whose upper levels are above-the-continuum autoionizing states of C II, which are generally considered to be excited by DR. Fortunately, there are a number of such transitions in the visible region that are detected in J0608. These include multiplets $\lambda\lambda 4010 - 4021$ ($^4S-^4P^o$), $\lambda\lambda 7046 - 7064$ ($^4S-^4P^o$), $\lambda\lambda 5479 - 5490$ ($^4D^o-^4D$), $\lambda\lambda 5250 - 5260$ ($^4F^o-^4D$), and $\lambda\lambda 4313 - 4326$ ($^4P-^4P^o$)

among the quartet states, and multiplets $\lambda\lambda 6095-6103$ ($^2P-^2D^\circ$), $\lambda\lambda 4960-4965$ ($^2P-^2P^\circ$), and $\lambda\lambda 8794-8800$ ($^2D-^2F^\circ$) among the doublet states.

DR coefficients have been published for only some of the above multiplets, so a comparison between observed and predicted relative intensities of C II multiplets that are likely due to recombination is confined to a limited sample of lines. The intensities of relevant C II multiplets are tabulated in Table 2, together with values predicted for radiative recombination (RR) for the doublets, and DR for the quartets at $T_e = 10^4$ K. The DR values calculated for the quartets include the excitation of C III into its lowest excited level, $2p\ ^3P^\circ$, for that temperature. The table also includes emission lines in the PN IC 418, where lower densities of $n_e \sim 10^4\text{ cm}^{-3}$ make it a useful comparison with the J0608 wind. No extinction correction has been applied for J0608 intensities, as the strong blue continuum and the location-based value of $E(B - V) = 0.09$ for its line of sight out of the Galaxy are both suggestive of small reddening.

A comparison of the doublet intensities observed in J0608 with those predicted for radiative recombination shows disagreements by factors of up to three among the different lines, and in the sense that all of the observed lines are stronger than predicted relative to $\lambda 4267$. This is indicative that recombination is not the only operative process populating the upper levels of C^+ . Several of the autoionization multiplets that are detected in the spectrum originate on levels ~ 2 eV above the C II ionization limit, which requires that the emission region kinetic electron temperature must be of order $T_e \geq 10^{3.6}$ K (Storey & Sochi 2013) if DR is the primary process populating the autoionizing levels. The fact that specific lines from highly excited doublet and quartet states have significant absorption components indicates large optical depth for those lines and is evidence of a large population of highly excited levels. Unusual for emission-line objects, this is difficult to achieve if only recombination, with its relatively small cross sections compared to collisional processes, is populating the levels.

It is notable that the P Cyg C II profiles in J0608 are present in the quartet but not the doublet states. Examination of Table 2 shows the observed intensities of the J0608 quartet transitions, relative to the doublets, to be significantly greater than predicted from DR. Some of the quartet multiplets show significant absorption, which is rarely observed and indicative of appreciable optical depth in these lines with their high excitation potentials. These facts indicate the quartet states are populated by a process other than solely DR, and, given their excitation potentials of ≥ 18 eV, it is unlikely to be collisional excitation from the ground state. The relatively high density of the wind line-emitting region indicated by the O I $\lambda 7773$ strength relative to $\lambda 8446$, suggests that collisional transfer is occurring from doublet levels to quartet states of similar excitation potential.

With one exception, C II multiplet 24, the line intensities for the PN IC 418 (Table 2) show quite good agreement with values predicted by radiative and dielectronic recombination. In contrast, for J0608 the doublet states are populated by a process in addition to radiative recombination.

An alternative excitation process to consider is radiative fluorescence from scattering of H and He resonance lines, especially since this is known to be an important process in PNe (Bowen 1934), active galactic nuclei (Weymann & Williams 1969), novae (Strittmatter et al. 1977), and compact X-ray sources (Margon & Cohen 1978). Coincidence in the wavelengths of resonance lines belonging to different ions produces a strong coupling between excitation of certain ions. Any fluorescence process between different ions almost certainly is initiated by line or continuum absorption from the ground state, which therefore strongly favors population of the C II doublet levels. However, in searching for wavelength overlaps between He I and C II resonance lines we find no clear coincidences likely to produce significant transfer of line radiation between those two ions.

Excitation of high levels, both bound and autoionizing, can occur from the absorption of UV continuum radiation such that absorption of continuum radiation by resonance lines is a plausible source of the J0608 emission line spectrum. Such absorption enables the direct excitation of autoionizing states of C II, inasmuch as radiative absorption from the ground state via two-electron excitation is allowed with f -values approaching $f = 0.01$ (van Hoof 2018; Kramida et al. 2018). Strong continuum radiation in the 500–600 Å region can pump C II autoionizing doublet states directly, with collisional transfer to quartet states possible at the high wind densities before autoionization or stabilizing radiative decay.

In summary, without detailed calculations it is difficult to make definite statements about the processes that produce the J0608 emission spectrum. Certainly, H is depleted with respect to He, and C is enhanced. The extent of carbon enhancement depends on the degree to which radiative absorption processes dominate recombination in populating excited doublet levels, which in turn collisionally populate the quartet levels. Future abundance determinations from strong C II emission spectra originating in stellar winds should take these processes into account and not rely solely on recombination as the primary excitation mechanism (e.g., Peña et al. 1997, Aleman et al. 2019).

Finally, we call attention to the presence of absorption lines in the J0608 spectrum that are not associated with accompanying emission. These lines occur predominantly in the spectrum shortward of 5200 Å, i.e., in the region where the continuum becomes increasingly strong into the blue. There are precedents for such absorption in late [WC] spectra that originate in the [WC] photosphere and are not fully obscured by the stellar wind (Crowther et al. 1998). The most definite of these features in other [WC] stars occur at wavelengths of 6146.66, 5596.95, 5806.14 and 5816.79; 4652.1 and 4654.2; and 8029.2 Å. We identify the $\lambda\lambda$ 5806, 5817 absorption with the C IV $\lambda\lambda$ 5801.35, 5811.97 doublet, and others as O III 5592.3 and the C III 4647.4, 4650.2, 4651.5 complex. These have been identified previously in a late [WC] star (Cohen & Jones 1987). Additionally, as noted in §8, there are a number of absorption features that are identified with O II and Ne II, as listed in Table 1.

The structure of the J0608 emitting region is clearly complex. Both collisional transfer between states and fluorescence are likely to be responsible for the strength of C II emission, and a high density is indicated for the wind, in agreement with the presence of O I λ 7773, λ 8446 (well-known to be due to resonance fluorescence), requiring $n > 10^{11}$ cm⁻³. On the other hand, the prominent forbidden emission of O, N, and S requires low density, so an undetected PN may well explain the presence of these latter lines. A fuller understanding of the physical conditions that produce the spectra of [WC] stars awaits detailed models that incorporate the processes that populate the different levels contributing to the emission.

10. CONCLUSIONS

J0608 is a new member of the rare [WC11] class, and likely the first such extragalactic member, thus with an accurately determined luminosity due to LMC membership. It is probably the central star of a PN, as are all other known [WC 11] stars, although no nebulosity is currently detected. As the prototype [WC11] star, CPD -56° 8032, at an (approximately determined) distance of ~ 1.4 kpc (De Marco, Barlow, & Storey 1997), has a prominent PN extending to $\sim 7''$ from the central star (Chesneau et al. 2006), the lack of a detection in J0608 at the LMC distance is probably not concerning.

We present arguments that the complex C II emission spectrum of J0608 and others in its class is formed within the high-density region of a wind, as indicated by the presence of a strong O I λ 7773 P Cyg feature. A significant number of emission lines originate from autoionizing levels of C II and its quartet levels. Their relative intensities differ markedly from those calculated for dielectronic recombination. Collisional transfer between levels of similar excitation potential is important in populating states of different multiplicity, and fluorescence from the stellar continuum is suggested as a significant process that may account for the appreciable intensities of lines detected from C II quartet and autoionizing levels. The assumption of radiative and dielectronic recombination alone as the cause of the C II emission for this class of star may well overestimate the C abundance.

Observational selection clearly favors discovery of these stars in the PN phase, but J0608 lacks at least an easily visible nebulae, and also perhaps the most prominent spectral signature, strong [O III] emission. Nor is there large-amplitude photometric variability to draw attention to the object. Finally, narrow-band photometric surveys tuned to the normally strongest WC lines (Massey et al. 2017 and references therein) will fail to discover these objects. We conclude that the number of late-type [WC] stars, both Galactic and in the Local Group, could be substantially larger than presently known.

Table 1. Identification and Measurements of J0608 Spectral Lines

ID	Trans.	Type	2017 December 30				2019 May 3			
			$\lambda_{\text{observed}}$ (Å)	Rel. Flux (Rel. to H β) ^a	EW (Å)	RV ^c (km s ⁻¹)	$\lambda_{\text{observed}}$ (Å)	Rel. Flux (Rel. to H β) ^b	EW (Å)	RV ^c (km s ⁻¹)
C II 3165.5	² D ^o - ² P	em					3168.0	1.75		237
C II 3167.9	² D ^o - ² P	em					3170.3	0.95		227
He I 3187.7	³ S- ³ P ^o	P Cyg	3190.0	0.57	-0.19	217	3189.9	0.47	-0.18	207
		abs	3201.5		-0.15		3200.8		-0.13	

Table 1 continued on next page

Table 1 (continued)

ID	Trans.	Type	2017 December 30				2019 May 3			
			$\lambda_{\text{observed}}$ (Å)	Rel. Flux (Rel. to H β) ^a	EW (Å)	RV ^c (km s ⁻¹)	$\lambda_{\text{observed}}$ (Å)	Rel. Flux (Rel. to H β) ^b	EW (Å)	RV ^c (km s ⁻¹)
Ne II 3230.1	² D– ² D ^o	abs	3232.8		–0.24	251	3232.4		–0.19	214
		em	3236.4	0.34			3236.4	0.4		
		abs	3280.6		–0.27		3280.6		–0.22	
		em	3282.0	0.26			3281.8	0.36		
Ne II 3297.7	⁴ P– ⁴ D ^o	abs	3300.7		–0.17	273	3300.3		–0.12	237
		abs	3302.2		–0.02		3302.7		–0.07	
Ne II 3323.7	² P– ² P ^o	abs	3326.5		–0.22	253	3326.1		–0.27	217
Ne II 3327.2	⁴ P– ⁴ D ^o	abs	3330.0		–0.14	253	3329.8		–0.27	234
Ne II 3334.8	² D ^o – ⁴ P	abs	3337.6		–0.42	252	3337.3		–0.53	225
Ne II 3345.5	² D– ² P ^o	abs	3347.7		–0.31	197	3347.4		–0.32	170
		abs	3357.8		–0.28		3357.6		–0.33	
		em	3364.2	1.13			3364.0	1.38		
		abs	3370.2		–0.15		3370.3		–0.13	
Ne II 3378.2	² P– ² P ^o	abs	3381.0		–0.13	249	3380.4		–0.3	195
		abs	3391.8		–0.14		3391.2		–0.09	
		abs	3395.7		–0.09		3395.6		–0.1	
		abs	3420.4		–0.22		3420.2		–0.17	
He I 3447.3	¹ S– ¹ P ^o	abs	3449.8		–0.08	218	3449.8		–0.13	218
		abs	3473.7		–0.11		3472.8		–0.14	
		abs	3484.5		–0.23		3484.3		–0.28	
He I 3498.6	³ P ^o – ³ D	P Cyg	3500.5	0.38	–0.18	163	3500.3	0.46	–0.21	146
		abs	3514.6		–0.08		3514.7		–0.03	
		abs	3545.6		–0.11		3545.3		–0.18	
Ne II 3568.5	² D– ² F ^o	abs	3571.6		–0.16	261	3571.2		–0.21	227
Ne II 3574.6	² D– ² P ^o	abs	3577.6		–0.19	252	3577.3		–0.24	227
He I 3587.3	³ P ^o – ³ D	abs	3589.7		–0.16	201	3589.6		–0.16	192
		em	3593.7	0.25						
		em	3604.6	0.17						
		abs	3613.7		–0.04		3612.0		–0.04	
He I 3613.6	¹ S– ¹ P ^o	abs	3615.9		–0.05	191	3616.0		–0.08	199
		abs	3636.6		–0.23		3636.5		–0.28	
		abs	3667.1		–0.3		3666.7		–0.34	
		abs	3697.2		–0.34		3696.9		–0.47	
		em	3703.6	0.2						
		abs	3707.3		–0.19		3707.4		–0.16	
		abs	3712.9		–0.1		3712.5		–0.15	
[O II] 3726.0	⁴ S ^o – ² D ^o	em	3728.9	1.06		234	3728.7	0.85		217
[O II] 3728.8	⁴ S ^o – ² D ^o	em	3731.6	1.7		225	3731.5	1.3		217
		abs	3738.4		–0.14		3737.8		–0.12	

Table 1 continued on next page

Table 1 (continued)

ID	Trans.	Type	2017 December 30				2019 May 3			
			$\lambda_{\text{observed}}$ (Å)	Rel. Flux (Rel. to H β) ^a	EW (Å)	RV ^c (km s ⁻¹)	$\lambda_{\text{observed}}$ (Å)	Rel. Flux (Rel. to H β) ^b	EW (Å)	RV ^c (km s ⁻¹)
O II 3749.5	⁴ P- ⁴ S ^o	abs	3752.0		-0.31	200	3752.1		-0.36	208
		abs	3758.0		-0.27		3757.5		-0.2	
		abs	3769.5		-0.18		3769.1		-0.23	
Si III 3796.1	³ P ^o - ³ D	em	3799.6	0.6		277	3799.2	0.48		245
		em	3805.6	0.27			3805.4	0.22		
Si III 3806.6	³ P ^o - ³ D	em	3809.8	0.38		252	3809.5	0.25		229
He I 3818.9	³ P ^o - ³ D	abs	3822.0		-0.31	244	3822.0		-0.27	244
C II 3831.7	² P ^o - ² D	em	3834.8	0.64		243	3834.6	0.55		227
C II 3835.7	² P ^o - ² D	em	3839.2	0.88		274	3839.0	0.68		258
& H9	& 2-9	em	3851.7	0.37						
		em	3858.6	0.24			3858.5	0.3		
		em	3880.4	0.72						
He I 3888.6	³ S- ³ P ^o	P Cyg	3891.3	1.87	-0.3	208	3891.3	2.0	-0.18	208
C II 3919.0	² P ^o - ² S	em	3922.3	1.18		253	3922.0	0.91		230
C II 3920.7	² P ^o - ² S	em	3924.0	2.2		253	3923.8	1.6		237
		em	3927.1	0.25			3926.9	0.3		
		em	3932.1	0.24			3931.9	0.33		
O II 3954.4	² P- ² P ^o	abs	3957.2		-0.29	212	3957.2		-0.37	212
He I 3964.7	¹ S- ¹ P ^o	P Cyg	3967.5	0.15	-0.14	212	3967.4	0.18	-0.11	204
He I	2-7	em	3973.4	0.14		251	3973.1			229
O II 3973.3	² P- ² P ^o	abs	3976.1		-0.25	211	3976.2		-0.33	219
		em	3983.3	0.18			3983.3	0.13		
		em	3988.3	0.09			3988.3	0.1		
He I 4009.3	¹ P ^o - ¹ D	P Cyg	4011.7	<0.01	-0.12	180	4012.3	0.08	-0.17	225
		em	4019.4	0.36			4019.0	0.2		
He I 4026.2	³ P ^o - ³ D	P Cyg	4029.5	0.94	-0.41	246	4029.4	1.08	-0.37	238
		em	4105.3	0.22		261	4105.0	0.25		239
He I 4120.8	³ P ^o - ³ S	abs	4123.4		-0.11	189	4123.0		-0.18	160
		em	4126.9	0.11			4126.8	0.12		
		em	4131.9	0.27			4131.8	0.29		
		em	4135.1	0.46			4134.9	0.31		
He I 4143.8	¹ P ^o - ¹ D	abs	4146.0		-0.2	159	4146.0		-0.23	159
		em	4159.6	0.17			4159.4	0.12		
		em	4211.4	0.28			4211.1	0.2		
		em	4214.7	0.27			4214.5	0.31		
		abs	4224.6		-0.19					
C II 4267.3	² G- ⁴ F ^o	em	4270.9	3.83		253	4270.7	3.43		239
C II 4292.3	² F ^o - ² G	em	4295.8	0.28		245	4295.6	0.29		231

Table 1 continued on next page

Table 1 (continued)

ID	Trans.	Type	2017 December 30				2019 May 3			
			$\lambda_{\text{observed}}$ (Å)	Rel. Flux (Rel. to H β) ^a	EW (Å)	RV ^c (km s ⁻¹)	$\lambda_{\text{observed}}$ (Å)	Rel. Flux (Rel. to H β) ^b	EW (Å)	RV ^c (km s ⁻¹)
C II 4306.3	² P ^o - ² S	em	4310.3	0.37		279	4310.1			265
O II 4317.1	⁴ P- ⁴ P ^o	abs	4320.1		-0.13	209	4320.1		-0.31	209
O II 4319.6	⁴ P- ⁴ P ^o	abs	4323.0		-0.22	236	4322.9		-0.36	229
C II 4329.8	² D- ² F ^o	em	4333.4	0.31		249	4333.2	0.44		236
O II 4336.9	⁴ P- ⁴ P ^o	abs	4339.8		-0.05	201	4340.0		-0.11	214
H γ	2-5	em	4344.0	0.28		244	4343.8	0.29		231
O II 4345.6	⁴ P- ⁴ P ^o	abs	4348.6		-0.21	207	4348.9		-0.31	228
O II 4349.4	⁴ P- ⁴ P ^o	abs	4352.5		-0.35	214	4352.6		-0.34	221
O II 4366.9	⁴ P- ⁴ P ^o	abs	4369.8		-0.36	199	4370.0		-0.47	213
C II 4372.4	⁴ P ^o - ⁴ D	em	4375.9	0.18		240	4375.6	0.18		220
C II 4375.0	⁴ P ^o - ⁴ D	em	4378.3	0.17		226	4378.3	0.08		226
C II 4376.6	⁴ P ^o - ⁴ D	em	4379.8	0.3		219	4379.7	0.18		213
He I 4387.9	¹ P ^o - ¹ D	abs	4390.6		-0.34	185	4390.6		-0.31	185
C II 4411.3	² D ^o - ² F	em	4414.4	0.59		211	4414.2	0.63		197
O II 4414.9	² P- ² D ^o	abs	4418.4		-0.33	238	4418.3		-0.34	231
O II 4417.0	² P- ² D ^o	abs	4420.2		-0.16	217	4420.4		-0.25	231
		em	4456.8	0.16			4457.0	0.1		
		em	4460.6	0.17			4460.5	0.21		
He I 4471.5	³ P ^o - ³ D	P Cyg	4474.8	0.5	-0.34	221	4474.5	0.53	-0.13	201
C II 4491.2	² F ^o - ² G	em	4495.0	0.32		254	4494.7	0.29		234
		abs	4519.9		-0.15		4519.6		-0.17	
O II 4591.0	² D- ² F ^o	abs	4594.2		-0.19	209	4594.4		-0.27	222
O II 4596.0	² D- ² F ^o	abs	4599.3		-0.19	215	4599.4		-0.29	222
C II 4619.2	² F ^o - ² G	em	4623.4	0.92		273	4623.2	0.74		260
C II 4637.6	² P ^o - ² D	em	4641.1	0.17		226	4640.9	0.29		214
O II 4641.8	⁴ P- ⁴ D ^o	abs	4645.2		-0.52	220	4645.1		-0.61	213
O II 4649.1	² F- ⁴ D ^o	abs	4652.2		-1.14	200	4652.6		-0.85	226
O II 4650.8	⁴ P- ⁴ D ^o	abs	4654.2		-0.57	219	4654.4		-0.39	232
O II 4661.6	⁴ P- ⁴ D ^o	abs	4664.7		-0.2	200	4664.9		-0.22	212
O II 4676.2	⁴ P- ⁴ D ^o	abs	4679.2		-0.2	193	4679.6		-0.17	218
		em	4700.2	0.2			4699.9	0.14		
He I 4713.2	³ P ^o - ³ S	P Cyg	4716.5	0.26	-0.07	210	4716.4	0.29	-0.04	204
C II 4735.5	² P- ² P ^o	em	4739.5	0.34		253	4739.1	0.25		228
C II 4738.0	² P- ² P ^o	em	4741.9	0.67		247	4741.6	0.79		228
C II 4744.8	² P- ² P ^o	em	4748.7	1.11		247	4748.5	1.14		234
C II 4747.3	² P- ² P ^o	em	4751.1	0.35		240	4750.8	0.43		221
		em	4756.7	0.29			4756.5	0.43		
		em	4760.4	0.36			4760.3	0.48		
C II 4802.7	² F ^o - ² G	em	4806.4	0.41		231	4806.2	0.41		219

Table 1 continued on next page

Table 1 (continued)

ID	Trans.	Type	2017 December 30				2019 May 3			
			$\lambda_{\text{observed}}$ (Å)	Rel. Flux (Rel. to H β) ^a	EW (Å)	RV ^c (km s ⁻¹)	$\lambda_{\text{observed}}$ (Å)	Rel. Flux (Rel. to H β) ^b	EW (Å)	RV ^c (km s ⁻¹)
C II 4862.6 & H β	² S- ² P ^o & 2-4	em	4865.6	1.0		185	4865.5	1.0		179
C II 4867.1	² S- ² P ^o	em	4870.8	0.23		228	4870.6	0.28		216
He I 4921.9	¹ P ^o - ¹ D	P Cyg	4925.5	0.14	-0.42	219	4925.3	0.17	-0.34	207
		em	4944.9	0.09			4944.7	0.06		
C II 4953.9	² P- ² P ^o	em	4957.7	0.16		230	4957.5	0.22		218
C II 4958.7	² P- ² P ^o	em	4963.2	0.23		272	4962.9	0.26		254
C II 4964.7	² P- ² P ^o	em	4968.7	0.44		242	4968.5	0.46		230
He I 5015.7	¹ S- ¹ P ^o	P Cyg	5019.1	0.85	-0.29	203	5019.0	0.88	-0.17	197
C II 5032.1	² P ^o - ² D	em	5036.2	0.57		244	5035.8	0.44		221
C II 5035.9	² P ^o - ² D	em	5039.9	0.53		238	5039.6	0.48		220
C II 5040.7	² P ^o - ² D	em	5044.9	0.25		250	5044.6	0.31		232
C II 5044.4	⁴ D ^o - ⁴ P	em	5048.3	0.21		232	5048.3	0.19		232
He I 5047.7	¹ P ^o - ¹ S	em	5052.0	0.17		256	5052.0	0.16		256
C II 5114	² P ^o - ² D	em	5118.1	0.56		241	5117.9	0.62		229
C II 5120.1	² P ^o - ² P	em	5124.0	0.4		229	5123.5	0.16		199
C II 5121.8	² P ^o - ² P	em	5126.1	0.47		252	5125.7	0.35		228
C II 5125.2	² P ^o - ² P	em	5129.4	0.11		246	5129.1	0.12		228
C II 5132.9	⁴ P ^o - ⁴ P	abs	5136.2		-0.34	193	5136.2		-0.28	193
C II 5133.3	⁴ P ^o - ⁴ P	em	5138.0	0.27		275	5137.8	0.27		263
C II 5137.3	⁴ P ^o - ⁴ P	em	5141.8	0.3		263	5141.4	0.12		239
C II 5139.2	⁴ P ^o - ⁴ P	em	5143.5	0.35		251	5143.4	0.2		245
C II 5143.5	⁴ P ^o - ⁴ P	abs	5146.7		-0.26	187	5146.7		-0.09	187
C II 5145.2	⁴ P ^o - ⁴ P	P Cyg	5149.2	0.24	-0.09	233	5149.1	0.22	-0.09	227
C II 5151.1	⁴ P ^o - ⁴ P	P Cyg	5154.9	0.21	-0.24	221	5154.9	0.17	-0.15	221
C II 5332.9	² P ^o - ² S	em	5337.1	0.3		236	5336.6	0.13		208
C II 5334.8	² P ^o - ² S	em	5338.9	0.36		231	5338.5	0.32		208
C II 5342.4	² F ^o - ² G	em	5346.7	0.43		242	5346.4	0.4		225
		em	5372.6	0.23			5372.3	0.2		
		em	5375.4	0.06			5374.6	0.13		
		em	5379.5	0.14			5378.9	0.06		
C IV 5411.4 & He II 5411.5	² G- ² H ^o & 4-7	abs	5416.8		-0.03	299	5415.9		-0.07	249
		em	5483.0	0.12			5482.7	0.09		
O III 5508.2	¹ D- ¹ D ^o	em	5513.2		-0.06	272	5512.6		-0.05	240
C II 5535.4	² S- ² P ^o	em	5540.4	1.04		271	5539.5	0.29		222
C II 5537.6	² S- ² P ^o	em	5541.8	0.45		228	5541.8	0.34		228
O III 5592.3	¹ P ^o - ¹ P	abs	5597.0		-0.27	252	5596.3		-0.29	215
C II 5640.5	⁴ P ^o - ⁴ S	em	5645.4	0.3		261	5645.2	0.22		250

Table 1 continued on next page

Table 1 (continued)

ID	Trans.	Type	2017 December 30				2019 May 3			
			$\lambda_{\text{observed}}$ (Å)	Rel. Flux (Rel. to H β) ^a	EW (Å)	RV ^c (km s ⁻¹)	$\lambda_{\text{observed}}$ (Å)	Rel. Flux (Rel. to H β) ^b	EW (Å)	RV ^c (km s ⁻¹)
C II 5648.1	⁴ P ^o - ⁴ S	P Cyg	5652.1	0.23	-0.06	213	5651.9	0.25	-0.05	202
C II 5662.5	⁴ P ^o - ⁴ S	P Cyg	5666.6	0.25	-0.12	217	5666.5	0.18	-0.08	212
C III 5695.9	¹ P ^o - ¹ D	em	5700.7	0.15		253	5701.3	0.05		284
		em	5744.4	0.06			5744.2	0.07		
C IV 5801.4	² S- ² P ^o	abs	5806.2		-0.21	248	5805.5		-0.24	212
C IV 5812.0	² S- ² P ^o	abs	5816.9		-0.26	253	5816.2		-0.15	217
C II 5818.3	⁴ D- ⁴ P ^o	em	5823.1	0.06		248	5822.4	0.06		211
C II 5823.2	⁴ D- ⁴ P ^o	em	5827.6	0.09		227	5827.4	0.08		216
C II 5827.9	⁴ D- ⁴ P ^o	em	5832.4	0.09		232	5832.2	0.1		221
C II 5836.4	⁴ D- ⁴ P ^o	em	5841.0	0.11		236	5840.6	0.14		216
C II 5843.6	⁴ D- ⁴ P ^o	em	5848.6	0.07		257	5848.4	0.15		246
C II 5856.1	⁴ D- ⁴ P ^o	em	5860.9	0.18		246	5860.5	0.21		225
He I 5875.6	³ P ^o - ³ D	P Cyg	5879.6	1.77	-0.33	204	5879.4	1.77	-0.13	194
C II 5889.8	² D- ² P ^o	em	5895.2	2.81		275	5894.8	2.71		255
C II 5907.2	⁴ P ^o - ⁴ S	em	5911.9	0.07		239	5911.6	0.09		224
C II 5914.6	⁴ P ^o - ⁴ S	em	5919.8	0.08		264	5919.3	0.11		238
		em	6011.5	0.06			6011.2	0.11		
		em	6024.6	0.07			6024.3	0.08		
		em	6039.1	0.04			6038.6	0.04		
		em	6042.0	0.08			6041.9			
		em	6067.2	0.06			6067.0	0.08		
		em	6083.5	0.06			6083.2	0.09		
C II 6095.3	² P- ² D ^o	em	6100.5	0.63		256	6100.0	0.34		231
C II 6098.5	² P- ² D ^o	em	6103.4	0.52		241	6103.1	0.57		226
C II 6102.6	² P- ² D ^o	em	6107.4	0.22		236	6107.4	0.15		236
		em	6118.8	0.08			6118.7	0.09		
C II 6151.5	² D- ² F ^o	em	6156.5	0.67		244	6156.2	0.59		229
		em	6172.3	0.08			6171.9	0.16		
		em	6181.0	0.05			6180.8	0.08		
		em	6218.0	0.12			6218.0	0.12		
C II 6251.1	² F ^o - ² G	em	6256.2	0.15		245	6255.8	0.15		226
C II 6257.2	² P ^o - ² D	em	6262.3	0.4		245	6261.8	0.22		221
C II 6259.6	² P ^o - ² D	em	6264.5	0.51		235	6264.1	0.55		216
		em	6284.9	0.06			6284.7	0.08		
[O I] 6300.3	³ P- ¹ D	em	6305.2	0.12		233	6305.0	0.1		224
Si II 6347.1	² S- ² P ^o	em	6351.6	0.18		213	6351.2	0.27		194
& Mg II 6346.8	& ² D- ² F ^o	em	6362.4	0.03			6362.0	0.03		
		em	6365.1	0.01						

Table 1 continued on next page

Table 1 (continued)

ID	Trans.	Type	2017 December 30				2019 May 3			
			$\lambda_{\text{observed}}$ (Å)	Rel. Flux (Rel. to H β) ^a	EW (Å)	RV ^c (km s ⁻¹)	$\lambda_{\text{observed}}$ (Å)	Rel. Flux (Rel. to H β) ^b	EW (Å)	RV ^c (km s ⁻¹)
		em	6367.7	0.04						
[O II] 6363.8	³ P- ¹ D	em	6368.4	0.09		217	6368.3	0.15		212
Si II 6371.0	² S- ² P ^o	em	6376.4	0.06		254	6376.2	0.09		245
		em	6388.6	0.11			6388.1	0.07		
		em	6390.0	0.07			6390.2	0.07		
		em	6397.4	0.06			6397.2	0.09		
		em	6407.8	0.06			6407.5	0.09		
		em	6430.2	0.11			6429.9	0.11		
C II 6462.0	² F ^o - ² G	em	6467.2	0.63		241	6466.7	0.36		218
		em	6511.8	0.04			6511.6	0.07		
		em	6527.4	0.05			6526.9	0.05		
[N II] 6548.0	³ P- ¹ D	em	6553.4	0.12		247	6552.9	0.11		225
H α	2-3	em	6568.1	2.16		242	6567.7	1.84		224
C II 6578.1	² S- ² P ^o	P Cyg	6582.6	1.61	-0.4	205	6582.4	1.74	-0.55	196
C II 6582.9	² S- ² P ^o	em	6588.7	2.58		264	6588.3	2.28		246
& [N II] 6583.5	& ³ P- ¹ D									
		em	6604.1	0.09			6603.8	0.12		
		em	6623.1	0.15			6622.9	0.18		
		em	6626.9	0.13			6626.7	0.16		
		em	6673.7	0.07			6673.3	0.15		
He I 6678.2	¹ P ^o - ¹ D	P Cyg	6682.9	0.61	-0.61	211	6682.7	0.69	-0.19	202
[S II] 6716.4	⁴ S ^o - ² D ^o	em	6722.1	0.27		255	6721.9	0.33		246
		em	6729.3	0.22			6729.0	0.23		
C II 6727.3	⁴ D- ⁴ D ^o	em	6732.8	0.04		245	6732.2	0.05		219
[S II] 6730.8	⁴ S ^o - ² D ^o	em	6736.4	0.19		250	6736.2	0.23		241
C II 6733.6	⁴ D- ⁴ D ^o	em	6738.8	0.05		232	6739.0	0.11		241
C II 6738.6	⁴ D- ⁴ D ^o	em	6744.3	0.07		254	6744.0	0.1		240
C II 6742.4	⁴ D- ⁴ D ^o	em	6748.2	0.09		258	6747.7	0.18		236
C II 6750.5	⁴ D- ⁴ D ^o	em	6756.5	0.1		267	6756.3	0.1		258
C II 6755.2	⁴ D- ⁴ D ^o	em	6760.8	0.04		249	6760.6	0.05		240
		em	6767.4	0.03						
C II 6780.6	⁴ P ^o - ⁴ D	P Cyg	6785.2	0.15	-0.37	204	6785.2	0.21	-0.24	204
C II 6783.9	⁴ P ^o - ⁴ D	em	6789.9	0.23		265	6789.8	0.22		261
C II 6787.2	⁴ P ^o - ⁴ D	em	6793.2	0.18		265	6793.0	0.16		256
C II 6791.5	⁴ P ^o - ⁴ D	em	6797.6	0.18		270	6797.3	0.15		256
C II 6798.1	⁴ P ^o - ⁴ D	em	6803.7	0.09		247	6803.5	0.12		238
C II 6800.7	⁴ P ^o - ⁴ D	em	6806.6	0.2		260	6806.4	0.13		251
C II 6812.3	⁴ P ^o - ⁴ D	em	6818.1	0.17		255	6817.6	0.12		233
		em	6827.2	0.11						

Table 1 continued on next page

Table 1 (continued)

ID	Trans.	Type	2017 December 30				2019 May 3			
			$\lambda_{\text{observed}}$ (Å)	Rel. Flux (Rel. to H β) ^a	EW (Å)	RV ^c (km s ⁻¹)	$\lambda_{\text{observed}}$ (Å)	Rel. Flux (Rel. to H β) ^b	EW (Å)	RV ^c (km s ⁻¹)
		em	6881.3	0.11			6826.8	0.11		
		em	6889.0	0.04			6831.8	0.03		
		em	6912.2	0.09			6911.7	0.14		
		em	6916.1	0.05			6915.7	0.11		
		em	6927.1	0.08			6927.0	0.11		
		em	6935.9	0.12			6935.5	0.14		
		em	7000.0	0.03			6999.8	0.03		
C III 7037.3	¹ P ^o - ¹ D	em	7043.0	0.09		243	7042.8	0.05		235
C II 7046.3	⁴ S- ⁴ P ^o	em	7051.9	0.12		238	7051.6	0.11		226
C II 7053.1	⁴ S- ⁴ P ^o	em	7058.8	0.22		242	7058.5	0.2		230
He I 7065.2	³ P ^o - ³ S	em	7071.2	1.03		255	7070.9	1.23		242
		em	7108.3	0.14			7108.0	0.1		
C II 7112.5	⁴ D- ⁴ F ^o	em	7118.4	0.11		249	7118.1	0.13		236
C II 7115.6	⁴ D- ⁴ F ^o	em	7121.1	0.14		232	7121.0	0.14		228
C II 7119.9	⁴ D- ⁴ F ^o	em	7125.8	0.22		249	7125.6	0.17		240
C II 7125.7	⁴ D- ⁴ F ^o	em	7131.5	0.08		244	7131.2	0.09		232
C II 7134.1	⁴ D- ⁴ F ^o	em	7139.7	0.15		236	7139.2	0.18		215
		em	7166.0	0.08			7165.7	0.12		
C II 7231.3	² P ^o - ² D	em	7237.4	2.9		253	7236.9	2.15		232
C II 7236.4	² P ^o - ² D	em	7242.6	3.53		257	7242.3	3.13		245
		em	7273.6	0.13			7273.1	0.14		
		em	7282.9	0.04						
He I 7281.4	¹ P ^o - ¹ S	em	7287.4	0.29		247	7287.0	0.24		231
[O II] 7320.0	² D ^o - ² P ^o	em	7325.5	0.11		225	7325.2	0.1		213
[O II] 7329.7	² D ^o - ² P ^o	em	7336.2	0.06		266	7335.7	0.11		246
		em	7376.1	0.05			7375.8	0.06		
		em	7439.5	0.05			7439.1	0.05		
		em	7465.3	0.02						
		em	7472.1	0.01						
		em	7475.5	0.08			7475.2	0.11		
C II 7505.3	² P ^o - ² D	em	7511.3	0.21		240	7510.8	0.18		220
C II 7508.9	² P ^o - ² P	em	7515.6	0.21		268	7515.1	0.2		248
C II 7520	² P ^o - ² P	em	7525.9	0.27		235	7525.6	0.3		223
		em	7530.0	0.05			7529.9	0.06		
C II 7530.6	² P ^o - ² P	em	7536.8	0.08		247	7536.3	0.08		227
		em	7571.0	0.03						
		em	7575.3	0.04						
		em	7580.3	0.12			7580.0	0.14		
O I 7771.9	⁵ S ^o - ⁵ P	abs	7776.6	0.15		181	7776.6		-0.5	181

Table 1 continued on next page

Table 1 (continued)

ID	Trans.	Type	2017 December 30				2019 May 3			
			$\lambda_{\text{observed}}$ (Å)	Rel. Flux (Rel. to H β) ^a	EW (Å)	RV ^c (km s ⁻¹)	$\lambda_{\text{observed}}$ (Å)	Rel. Flux (Rel. to H β) ^b	EW (Å)	RV ^c (km s ⁻¹)
O I 7775.4	⁵ S ^o - ⁵ P	P Cyg	7780.7	0.17		205	7780.7	0.2	-0.28	205
		em	7802.3	0.06			7802.0	0.04		
		em	7822.2	0.04						
		em	7867.1	0.13			7866.8	0.16		
		em	7883.4	0.05			7883.0	0.11		
		em	7902.7	0.07			7902.4	0.14		
C II 8037.7	⁴ P- ⁴ P ^o	em	8045.0	0.1		273	8044.6	0.13		258
C II 8062.1	⁴ P- ⁴ P ^o	em	8068.9	0.12		253	8068.5	0.14		238
C II 8076.6	⁴ P- ⁴ P ^o	em	8083.1	0.13		241	8082.7	0.11		227
		em	8146.7	0.11			8146.5	0.17		
		abs	8169.8		-0.44		8169.6		-0.35	
		abs	8178.2		-0.61		8178.0		-0.41	
C II 8214.5	² G- ² H ^o	em	8221.4	0.13		252	8221.0	0.2		237
		em	8240.6	0.05			8240.6	0.05		
		abs	8288.7		-0.32		8288.0		-0.28	
		abs	8294.6		-0.51		8294.2		-0.18	
		em	8300.2	0.31			8299.8	0.23		
		em	8341.9	0.03						
		em	8345.8	0.08			8345.4	0.06		
		em	8357.1	0.09			8356.6	0.13		
		em	8399.4	0.03						
		em	8417.0	0.02						
		em	8420.1	0.04						
em	8430.4	0.01								
O I 8446.4	³ S ^o - ³ P	em	8453.1	0.16		238	8452.8	0.28		227
C II 8682.5	² S- ² P ^o	em	8689.9	0.53		256	8689.5	0.6		242
C II 8696.7	² S- ² P ^o	em	8704.1	0.3		255	8703.7	0.36		242
		em	8801.8	0.45						
		em	8808.1	0.24						
		em	8827.4	0.07						
		em	8880.8	0.16			8880.2	0.15		
		em	8919.9	0.07						
		em	8958.8	0.1						
C II 9089.1	² G- ² H ^o	em	9096.6	0.06		248	9095.8	0.07		221
		em	9102.8	0.08						
		em	9225.7	0.09			9225.2	0.17		
		em	9231.0	0.09			9230.6	0.12		
C II 9229.6	² D- ² F ^o	em	9237.1	0.43		244	9236.9	0.44		237
		em	9243.8	0.17			9243.7	0.23		

Table 1 continued on next page

Table 1 (*continued*)

ID	Trans.	Type	2017 December 30				2019 May 3			
			$\lambda_{\text{observed}}$ (Å)	Rel. Flux (Rel. to H β) ^a	EW (Å)	RV ^c (km s ⁻¹)	$\lambda_{\text{observed}}$ (Å)	Rel. Flux (Rel. to H β) ^b	EW (Å)	RV ^c (km s ⁻¹)
C II 9904	² F ^o - ² G	em	9251.8	0.07			9251.3	0.11		
		em	9257.5	0.09			9257.3	0.1		
		em					9412.8	0.19		
		em					9857.6	0.26		
		em					9911.0	0.65		212
		em					10245.0	0.2		
He I 10830	³ S- ³ P ^o	em					10264.0	0.13		
		em					10838.9	0.59		247

^a2017 H β + C II blend flux is 5.0×10^{-15} erg s⁻¹ cm⁻² Å⁻¹

^b2019 H β + C II blend flux is 5.7×10^{-15} erg s⁻¹ cm⁻² Å⁻¹

^cAll quoted radial velocities are heliocentric, positive values.

NOTE—Table 1 is published in its entirety in the machine readable format. A portion is shown here for guidance regarding its form and content.

Table 2. C II Recombination Intensities

Line (Doublets)	RR Recombination Coeffs ^a	Predicted Recomb Intensity	Observed Intensity	
			J0608	IC 418 ^c
(Å)	($10^{-14} \text{ cm}^3\text{s}^{-1}$)	($F_{4267} = 100$)		
C II λ 4267	27.6	100.0	100.0	100
C II λ 5342	1.84	5.3	10.7	4.9
C II λ 6151	1.69	4.3	13.4	4.4
C II λ 6462	4.29	10.3	13.8	10.2
C II λ 9230	3.65	6.1	10.7	...
Line (Multiplets)	DR Recombination Coeffs ^b			
C II 6095-6103 (24)	0.17	0.43	39.0	0.19
C II 4372-4374 (45)	0.99	3.5	18.7	...
C II 7112-7134 (20)	1.33	2.9	27.0	2.9

^aRecombination coefficients are for $T_{\text{eff}} = 10^4$ K (Davey et al. 2000)

^bDielectronic recombination coefficients are for $T_{\text{eff}} = 10^4$ K (Sochi & Storey 2013)

^cIC 418 intensities from Sharpee et al. (2003)

We thank G. Ferland, G. Jacoby, P. Massey, M. Phillips, A. Pradhan, I. Soszynski, R. van der Marel, and K. Werner for useful discussions and data, and are grateful to N. Hambly for supplying the SuperCOSMOS images. We appreciate comments by the anonymous referee, which have improved this manuscript. This work has made use of data from the European Space Agency (ESA) mission *Gaia* (<https://www.cosmos.esa.int/gaia>), processed by the *Gaia* Data Processing and Analysis Consortium (DPAC, <https://www.cosmos.esa.int/web/gaia/dpac/consortium>). Funding for the DPAC has been provided by national institutions, in particular the institutions participating in the *Gaia* Multilateral Agreement.

REFERENCES

- Acker, A., & Neiner, C. 2003, *A&A*, 403, 659
- Aitken, D. K., Barlow, M. J., Roche, P. F., & Spenser, P. M. 1980, *MNRAS*, 192, 679
- Alcock, C., Allsman R. A., Alves, D. R., et al. 2001, *ApJ*, 554, 298
- Aleman, I., Leal-Ferreira, M. L., Cami, J., et al. 2019, *MNRAS*, in press
- Bhatia, A. K., & Kastner, S. O. 1995, *ApJS*, 96, 325
- Bidelman, W. P., MacConnell, D. J., & Bond, H. E. 1968, *IAUC* 2098
- Bond, H. E., & Ciardullo, R. 1991, in *ASP Conf. Ser.* 20, *Frontiers of Stellar Evolution: Celebrating the 50th Anniversary of McDonald Observatory*, ed. D. L. Lambert (San Francisco: ASP), 592
- Bowen, I. S. 1934, *PASP*, 46, 146
- Breysacher, J., Azzopardi, M., & Testor, G. 1999, *A&AS*, 137, 117
- Campbell, W. W. 1893, *PASP*, 5, 204
- Chesneau, O., Collioud, A., De Marco, O., et al. 2006, *A&A*, 455, 1009
- Choi, J., Dotter, A., Conroy, C., et al. 2016, *ApJ*, 823, 102
- Clayton, G. C., De Marco, O., Whitney, B. A., et al. 2011, *AJ*, 142, 54
- Clegg, R. E. S. 1989, in *IAU Symp.* 131, *Planetary Nebulae*, ed. S. Torres-Peimbert (Dordrecht: Kluwer), 139
- Cohen, M., & Jones, B. F. 1987, *ApJ*, 321, L151
- Cohen, M., Barlow, M. J., Sylvester, R. J., et al. 1999, *ApJL*, 513, L135
- Cooke, R. J., Pettini, M., Jorgenson, R. A., Murphy, M. T., & Steidel, C. C. 2014, *ApJ*, 781, 31
- Cowley, A. P., & Hiltner, W. A. 1969, *A&A*, 3, 372
- Crowther, P. A. 2008, in *Hydrogen-Deficient Stars*, eds. A. Werner & T. Rauch, *ASP Conf. Ser.*, 391, 83
- Crowther, P. A., De Marco, O., & Barlow, M. J. 1998, *MNRAS*, 296, 367
- Dahari, O., & Osterbrock, D. E. 1984, *ApJ*, 277, 648
- Davey, A. R., Storey, P. J., & Kisielius, R. 2000, *A&AS*, 142, 85
- De Araujo, F. X., Marcolino, W. L. F., Pereira, C. B., & Cuisinier, F. 2002, *AJ*, 124, 464

- De Marco, O. 2008, in *Hydrogen-Deficient Stars*, eds. A. Werner & T. Rauch, ASP Conf. Ser., 391, 209
- De Marco, O., Barlow, M. J., & Cohen, M. 2002, *ApJ*, 574, L83
- De Marco, O., Barlow, M. J., & Storey, P. J. 1997, *MNRAS*, 292, 86
- De Marco, O., & Crowther, P. 1998, *MNRAS*, 296, 419
- De Marco, O., Storey, P. J., & Barlow, M. J. 1997, *MNRAS*, 297, 1014
- DePew, K., Parker, Q. A., Miszalski, B., De Marco, O., Frew, D. J., Acker, A., Kovacevic, A. V., & Sharp, R. G. 2011, *MNRAS*, 414, 2812
- Dotter, A. 2016, *ApJS*, 222, 8
- Drake, S. A., & Ulrich, R. K. 1980, *ApJS*, 42, 351
- Fitzpatrick, E. L. 1999, *PASP*, 111, 63
- Gaia Collaboration, Brown, A. G. A., Vallenari, A., et al. 2018, *A&A*, 616, A1
- Geier, S., Raddi, R., Gentile Fusillo, N. P., & Marsh, T. R. 2019, *A&A*, 621, A38
- Górny, S. K. 2001, *Ap&SS*, 275, 67
- Górny, S. K. 2008, in *Hydrogen-Deficient Stars*, eds. A. Werner & T. Rauch, ASP Conf. Ser., 391, 165
- Górny, S. K., Stasinska, G., Szczerba, R., & Tylanda, R. 2001, *A&A*, 377, 1007
- Grindlay, J., Tang, S., Los, E., & Servillat, M. 2012, in *IAU Symp 285, New Horizons in Time-Domain Astronomy*, ed. R. E. M. Griffin, R. J. Hanisch, & R. Seaman (Cambridge: Cambridge Univ. Press), 29
- Guerrero, M. A., Fang, X., Miller Bertolami, M. M., et al. 2018, *Nature Astr.*, 2, 784
- Handler, G., Prinja, R. K., Urbaneja, M. A., Antoci, V., Twicken, J. D., & Barclay, T. 2013, *MNRAS*, 430, 2923
- Heber, U. 2001, *PASP*, 128, 082001
- Heck, A., Houziaux, L., Manfroid, J., Jones, D. H. P., & Andres, P. J. 1985, *A&AS*, 61, 375
- Helmi, A., van Leeuwen, F., McMillan, P. J., et al. 2018, *A&A*, 616, A12
- Henry, R. B. C., Kwitter, K. B., Jaskot, A. E., Balick, B., Morrison, M. A., & Milingo, J. B. 2010, *ApJ*, 724, 748
- Hrivnak, B. J., Lu, W., Volk, K., Szczerba, R., Soszyński, I., & Hajduk, M. 2015, *ApJ*, 805, 78
- Kaler, J. B. 1981, *ApJ*, 249, 201
- Kameswara Rao, N., Giridhar, S., & Nandy, K. 1990, *A&A*, 234, 410
- Kastner, S. O., & Bhatia, A. K. 1995, *ApJ*, 439, 346
- Kochanek, C. S., Shappee, B. J., Stanek, K. Z., et al. 2017, *PASP*, 129, 104502
- Kramida, A., Ralchenko, Yu., Reader, J., & NIST ASD Team (2018). NIST Atomic Spectra Database (version 5.6.1), <https://physics.nist.gov/asd>, National Institute of Standards and Technology, Gaithersburg, MD.
- Leisy, P., Dennefeld, M., Alard, C., & Guibert, J. 1997, *A&AS*, 121, 407
- Leuenhagen, U. & Hamann, W. R. 1994, *A&A*, 283, 567
- Lindgren, L., Lammers, U., Bastian, U., et al. 2016, *A&A*, 595, A4
- Manick, R., Miszalski, B., & McBride, V. 2015, *MNRAS*, 448, 1789
- Margon, B., & Cohen, J. G. 1978, *ApJ*, 222, L33
- Margon, B., Prochaska, J. X., Tejos, N., & Monroe, T. 2016, *PASP*, 128, 024201
- Marshall, J. L., Burles, S., Thompson, I. B., et al. 2008, *Proc. SPIE*, 7014, 54
- Massey, P., Neugent, K. F., & Morrell, N. 2017, *ApJ*, 837, 122
- Méndez, R. H. 1991, *Evolution of Stars: the Photospheric Abundance Connection (IAU Symp. 145)*, ed. G. Michaud, & A. V. Tutukov (Cambridge: Cambridge Univ. Press), 375
- Menzel, D. H., & Marshall, R. K. 1933, *PNAS*, 19, 879
- Miszalski, B., Mikołajewska, J., Köppen, J., et al. 2011, *A&A*, 528, A39
- Monroe, T. R., Prochaska, J. X., Tejos, N., Worseck, G., Hennawi, J. F., Schmidt, T., Tumlinson, J., & Shen, Y. 2016, *AJ*, 152, 25
- Morgan, D. H., & Good, A. R. 1992, *A&AS*, 92, 571
- Morgan, D. H. 1994, *A&AS*, 103, 235
- Nidever, Olsen, K., Choi, Y., et al. 2019, *ApJ*, 874, 118
- Parker, Q. A., Phillipps, S., Pierce, M. J., et al. 2005, *MNRAS*, 362, 689
- Peña, M. 2005, *RMxAA*, 41, 423
- Peña, M., Ruiz, M. T., & Torres-Peimbert, S. 1997, *A&A*, 324, 674
- Pickering, E. C. 1891, *Astr. Nach.*, 127, 1
- Schindewolf, M., Németh, P., Heber, U., Battisch, T., Bertolami, M. M. M., Irrgang, A., & Latour, M. 2018, *A&A*, 620, A36
- Schönberner, D. 1981, *A&A*, 103, 119
- Shappee, B. J., Prieto, J. L., Grupe, D., et al. 2014, *ApJ*, 788, 48
- Sharpee, B., Williams, R., Baldwin, J. A., & van Hoof, P. A. M. 2003, *ApJS*, 149, 157
- Smith, L. F., & Aller, L. H. 1971, *ApJ*, 164, 275
- Sochi, T., & Storey, P. J. 2013, *ADNDT*, 99, 633
- Soszyński, I., Udalski, A., Szymański, M. K., et al. 2009, *AcA*, 59, 335
- Storey, P. J., & Hummer, D. G. 1995, *MNRAS*, 272, 41

- Storey, P. J., & Sochi, T. 2013, *MNRAS*, 430, 599
- Strittmatter, P. A., Woolf, N. J., Thompson, R. I., et al. 1977, *ApJ*, 216, 23
- Sun, M., Jiang, B. W., Zhao, H., Gao, J., Gao, S., Jian, M., & Yuan, H. 2018, *ApJ*, 861, 153
- Tang, S., Grindlay, J., Los, E., & Servillat, M. 2013, *PASP*, 125, 857
- Thackeray, A. D. 1977, *Observatory*, 97, 165
- Torres, A. V., Conti, P. S., & Massey, P. 1986, *ApJ*, 300, 379
- Udalski, A., Szymański, M. K., & Szymański, G. 2015, *AcA*, 65, 1
- van Aarle, E., van Winckel, H., Lloyd Evans, T., et al. 2011, *A&A*, 530, A90
- van der Marel, R. P., Alves, D. R., Hardy, E., & Suntzeff, N. B. 2002, *AJ*, 124, 2639
- Van der Hucht, K. A., Conti, P. S., Lundström, I., & Stenholm, B. 1981, *SSRv*, 28, 227
- van Hoof, P. A. M. 2018, *Galaxies*, 6, 63
- Vasiliev, E. 2018, *MNRAS*, 481, L100
- Webster, B. L., & Glass, I. S. 1974, *MNRAS*, 166, 491 (“WG74”)
- Weidmann, W. A., & Gamen, R. 2011, *A&A*, 526, A6
- Weymann, R. J., & Williams, R. E. 1969, *ApJ*, 157, 1201
- Wolf, C., Onken, C. A., Luvaul, L. C., et al. 2018, *PASA*, 35, E010
- Zijlstra, A. A. 2001, *Ap&SS*, 275, 79